



Quasi-synoptic transport, budgets and water mass transformation in the Azores–Gibraltar Strait region during summer 2009



Lidia Isabel Carracedo Segade^{a,*}, Miguel Gilcoto^a, Herlé Mercier^b, Fiz Fernández Pérez^a

^a Marine Research Institute (IIM-CSIC), Eduardo Cabello 6, 36208 Vigo, Spain

^b CNRS, Laboratoire de Physique des Océans, Institut Français de Recherche pour l'Exploitation de la Mer (IFREMER), Centre de Brest, C.S. 1007029280 Plouzané, France

ARTICLE INFO

Article history:

Received 13 February 2014

Received in revised form 16 September 2014

Accepted 16 September 2014

Available online 28 September 2014

ABSTRACT

We describe the circulation patterns in the Azores–Gibraltar Strait region (North-Eastern Atlantic) during the 2009 CAIBOX cruise on the basis of hydrographic and direct current velocity measurements. This study offers new data for a region where importation of central waters (subpolar and subtropical modes of Eastern North Atlantic Central Water) and exports of Mediterranean Water are strongly related to large-scale dynamics in the North Atlantic Ocean (Azores Current–Mediterranean Water system). The description is backed up quantitatively by the results of a box inverse model, which was used to obtain absolute water mass transport values consistent with thermal wind equations and with conservation of volume, salt and heat. The contributions of water masses were determined in an extended Optimum Multiparameter Analysis from a quasi-synoptic point of view, providing detail in addition to volume, salt and heat transport.

The surface–subsurface large-scale current system in the region consists of the Azores Current (13.1 ± 2.5 Sverdrup [Sv], $1 \text{ Sv} = 10^6 \text{ m}^3 \text{ s}^{-1}$), the Azores Counter-Current (5.2 ± 2.1 Sv), the Portugal Current (4.5 ± 1.4 Sv) and the Canary Current (7.1 ± 1.1 Sv). Broadly speaking, central waters are imported into the CAIBOX region at a rate of 1.6 ± 0.9 Sv, and Mediterranean Water is exported at a rate of 1.5 ± 0.4 Sv. The downwelling of central waters west of Gibraltar Strait was quantified at 1.1 Sv. Not all this volume participates in MW formation, but 0.8 Sv of entrained central waters; of which 0.5 Sv are from central waters of subpolar origin and 0.3 Sv from subtropical central waters. Of the 4.9 Sv of subtropical central waters advected by the Azores Current, about 0.7 Sv would reach the Gulf of Cadiz region either to take part in central water entrainment or to flow across the Gibraltar Strait as part of the Atlantic inflow to the Mediterranean Sea.

© 2014 Elsevier Ltd. All rights reserved.

Introduction

The subtropical eastern North Atlantic is a region of eastern boundary ventilation (Barton, 1998; Arístegui et al., 2004; Álvarez

and Álvarez-Salgado, 2007) due in part to entrainment of central waters into Mediterranean Outflow Water (MOW) (van Aken, 2000; Álvarez et al., 2005; Fusco et al., 2008) and also to meridional spread and mixing of low-oxygen high-nutrient subtropical and recently ventilated subpolar central water modes (Ríos et al., 1992; Pérez et al., 2001). The former leads to an overturning circulation, whereby central waters enter the region and saltier, intermediate water flows out below, spreading to the Atlantic Ocean.

The easternmost surface current systems in the area (Fig. 1) are the Portugal Current (PC) system off the Iberian Peninsula and the Canary Current (CC) system off the African coast (Álvarez-Salgado et al., 2003). The former is fed by the south-westward branches of the North Atlantic Current (Paillet and Mercier, 1997; Pérez et al., 2001), while the latter is a natural extension (easternmost branch) of the Azores Current (AC) (Machín et al., 2006). The surface circulation in this region is subject to a seasonal wind cycle, i.e. the meridional shift of the trade winds system. Northerly winds predominate during summer (Fig. 1b), leading to seasonal upwelling

Abbreviations: AA, diluted form of Antarctic Bottom Water; AC, Azores Current; ACC, Azores Counter-Current; CC, Canary Current; CTD, Conductivity, Temperature and Depth; ENACW_p, Subpolar Eastern North Atlantic Central Water; ENACW_T, Subtropical Eastern North Atlantic Central Water; (e)OMP, (extended) Optimum Multiparameter Analysis; E – P – R, Evaporation minus Precipitation minus river Runoff; ERA40, European 45-year global atmospheric Re-Analysis; IPC, Iberian Poleward Current; ISOW, Iceland–Scotland Overflow Water; H, Harvey Water; LSW, Labrador Sea Water; MMW, Madeira Mode Water; MOW, Mediterranean Outflow Water; MW, Mediterranean Water; NEADW_L, North-East Atlantic Deep Water Lower; PC, Portugal Current; SADCP, Shipboard Acoustic Doppler Current Profiler; WOA09, World Ocean Atlas 2009.

* Corresponding author. Tel.: +34 986 231 930x363.

E-mail addresses: lcarracedo@iim.csic.es (L.I. Carracedo Segade), migil@iim.csic.es (M. Gil Coto), Herle.Mercier@ifremer.fr (H. Mercier), fiz.perez@iim.csic.es (F.F. Pérez).

off the western Iberian coast. Off the North African coast, however, they are almost continual all year round (Aristegui et al., 2004). The PC system consists of a weak branch offshore, known as PC, and a seasonally changing onshore compensating slope poleward current, known as the Iberian Poleward Current (IPC, Péliz et al., 2003, 2005; Relvas et al., 2007). The highest IPC flux is usually characterized in winter (Haynes and Barton, 1990; Mazé et al., 1997; Barton, 1998, 2001; van Aken, 2000; Pérez et al., 2001; Álvarez-Salgado et al., 2003; Péliz et al., 2003). During spring and summer, the IPC weakens and its core deepens and moves offshore (Péliz et al., 2003, 2005), while the southward transport of the PC is strengthened at the surface and over the slope by the wind-driven equatorward Portugal Coastal Current (Álvarez-Salgado et al., 1993; Castro et al., 1994, 2000; Pérez et al., 2001; Aristegui et al., 2004). The CC southward transport also appears to be enhanced during this part of the year, with the presence of a southward coastal jet, the Canary Upwelling Current (Pelegrí et al., 2005; Machín et al., 2006).

Numerous previous studies have provided quantification of North Atlantic circulation patterns with inverse (Mercier et al., 1993; Wunsch, 1994; Mazé et al., 1997; Paillet and Mercier, 1997; Slater, 2003; Álvarez et al., 2005; Hernández-Guerra et al., 2005; Machín et al., 2006; Álvarez and Álvarez-Salgado, 2009) and numerical (Batteen et al., 2000; Jia, 2000; Johnson and Stevens, 2000; New et al., 2001; Özgökmen et al., 2001; Jia et al., 2007; Péliz et al., 2007; Volkov and Fu, 2010; Bozec et al., 2011; Mason et al., 2011) models. Evaluation and quantification of the advective transport of physical parameters in the ocean is important not only to establish the corresponding volume, heat and salt budgets and to better determine the variability of the main current systems but also to further estimate chemical transports and budgets.

Of particular interest for comparison with the present study are studies in which box inverse models were used (based on thermal wind equations combined with mass, salinity and heat conservation within density layers) in the eastern North Atlantic. Mazé et al. (1997) described the circulation off west the Iberian Peninsula during a box-like cruise in May 1989. Hernández-Guerra et al. (2005) and Machín et al. (2006) performed similar measurements in the Canary Basin region, the former on a box-like cruise in

September 2003 and the latter during four seasonal cruises between 1997 and 1998. Slater (2003) and Álvarez et al. (2005) combined sections from different cruises to form non-synoptic boxes in the region delimited by the Azores Islands and the Gibraltar Strait; Álvarez et al. (2005) also combined the absolute velocities obtained from the inverse model with the results of a multiparameter mixing analysis of the water masses, as we did in this study. The most recent equivalent study is that of Pérez-Hernández et al. (2013), on a box-like cruise between the Azores and the Gibraltar Strait in October–November 2009.

The aim of this study was to make new observations and transport estimates to better characterize circulation in the north-eastern Atlantic region. As the central water transformation mechanisms are strongly linked to the dynamics of the region, we focused our analysis on the fate of central water masses. In order to characterize circulation in this area and to analyze central water transformation mechanisms, we used a two-dimensional inverse ocean model. Water mass mixing was resolved by use of an extended Optimum Multiparameter (eOMP) method.

Data and methods

Dataset

Field data were obtained during the CAIBOX cruise (25 July to 14 August 2009) on board the B/O *Sarmiento de Gamboa*. The survey comprised three large-scale conductivity, temperature and depth (CTD rosette) sections defining a box in the Iberian Basin: a north zonal one at 41°30'N, a west meridional one at 20°W and a south transverse that closed the box against the African coast through the Canary Islands (Fig. 1). During the cruise, 71 hydrographic stations were set up, at which multidisciplinary observations were carried out in the water column with a SBE911plus CTD rosette equipped with 24 Niskin bottles (12 L). At each station, profiles of temperature and salinity were obtained during the CTD downcast, while 24 pressure levels were sampled with Niskin bottles and CTD sensors on the upcast. The CTD data were processed by standard procedures and software from SeaBird. The CTD-derived salinity was calibrated with water samples collected with the CTD rosette and analyzed on board with a Guildline 8410-A

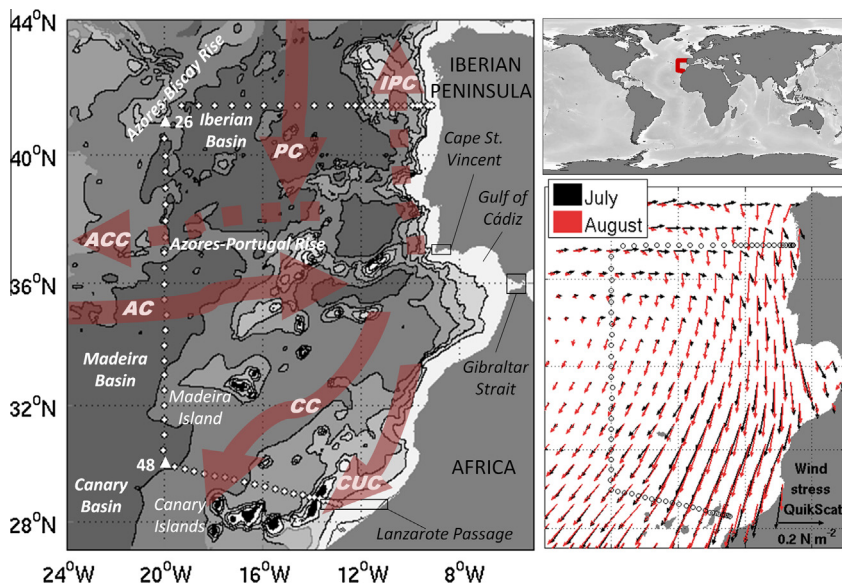


Fig. 1. CAIBOX cruise track (white dots) with north zonal section (stations 1–25), west meridional section (stations 26–48) and south transverse section (stations 48–71). The figure shows topographical features: Azores–Biscay Rise, Azores–Portugal Rise, Iberian Basin, Madeira Basin, Canary Basin and Gulf of Cadiz. Enclosure: July and August 2009 wind stress (N m^{-2}) fields.

Portasal. At two stations (40 and 47), the CTD did not get close to the bottom for technical reasons, and the downcast profiles were depth-interpolated (2571–5005 dbar and 2605–4164 dbar, respectively) from the results for nearby, deeper stations. Seawater samples were analyzed on board to determine dissolved oxygen concentration (O_2) and nutrients (nitrate plus nitrite [hereinafter nitrate, NO_3], phosphate [PO_4] and silicate [SiO_4]). The Winkler (1988) method was used to derive O_2 (Fajar et al., 2012), and nutrients were determined by standard segmented flow analysis with an Alpkem analyser (Álvarez-Salgado et al., 1992). These chemical properties were used in solving the water mass multiparameter mixing model. Potential temperature (θ), practical salinity spatial distributions and mean property profiles by section are shown in Fig. 2a, while θ/S diagrams by section are depicted in Fig. 2b.

Under-way velocity measurements between 10 and ~650 dbar were obtained with the Shipboard Acoustic Doppler Current Profiler (SADCP; RDI Ocean Surveyor at 75 kHz). Raw data were

averaged into 2-min files (short-term average) and then post-processed with Cascade 6.1 software (Le Bot et al., 2011), including ship velocity screening, tidal removal, quality flag assignment, data filtering and an alignment correction (0.4°) that minimizes the correlation between the ship's velocity and the current component along the trajectory. After processing, SADCP velocities were averaged for all stations, thus obtaining profiles at the station pair positions and diminishing the effect of ageostrophic dynamics.

Satellite-derived products, such as sea-level anomaly and geostrophic velocities, were used to show mesoscale eddy variation. The data come from the multi-mission altimetry products provided by Aviso (gridded delayed time “upd” products, <http://www.aviso.oceanobs.com/duacs/>) on a $1/3^\circ$ grid, with data every 7 days since October 1992. High-resolution QuikScat winds (Fig. 1, inset map, $0.5^\circ \times 0.5^\circ$, <http://cersat.ifremer.fr/>) for the year of the CAIBOX cruise (2009) were used to compute the Ekman transport induced by the wind drag on the sea surface. Another source of

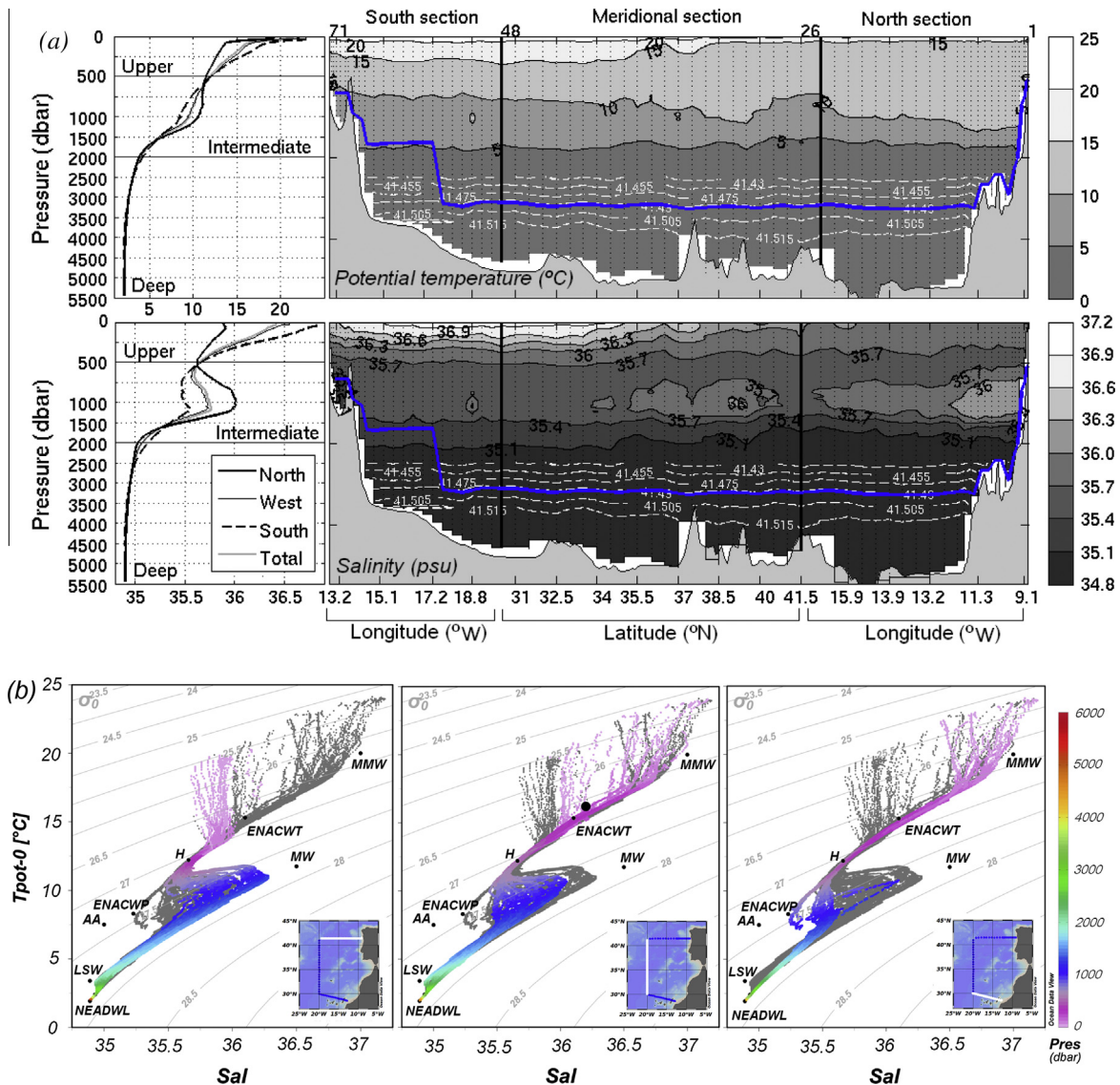


Fig. 2. (a) Vertical distributions of potential temperature (θ) and salinity (S) on the CAIBOX cruise. White isopycnals (σ_3 , $kg\ m^{-3}$) correspond to deep-layer limits used to constrain the model, and the blue line represents the reference level. (b) θ (surface reference level) vs. S of the CTD CAIBOX casts. Isolines correspond to potential density anomalies (σ_θ , $kg\ m^{-3}$). Black dots mark the positions of source water types, and the black circle the position of the Azores Front. Coloured dots corresponding to each section are displayed over the whole-cruise dots (in grey). The white line in the inset map marks the section for which θ/S points are displayed. H, Harvey limit point; MMW, Madeira Mode Water; ENACW_T, Subtropical Eastern North Atlantic Central Water; MW, Mediterranean Water; ENACW_P, Subpolar Eastern North Atlantic Central Water; AA, diluted form of Antarctic Intermediate Water; LSW, Labrador Sea Water; NEADWL, North-East Atlantic Deep Water Lower. (For interpretation of the references to colour in this figure legend, the reader is referred to the web version of this article.)

data was the European 40-year re-analysis of meteorological observations (ERA40), from September 1957 to August 2002, produced by the European Centre for Medium-range Weather Forecasts ($2.5^\circ \times 2.5^\circ$, <http://www.ecmwf.int/>), from which air–sea volume fluxes were extracted (evaporation, precipitation and river runoff).

The box inverse model: absolute velocity field and transports

An inverse model was used to compute absolute transport across CAIBOX sections, integrating thermal wind and property (volume and tracers, i.e. salinity and temperature) conservation equations to obtain property budgets in the box (see Mercier, 1986; Lux et al., 2001; Mercier et al., 2003; Lherminier et al., 2007, 2010 for further details). The resulting set of equations includes two types of unknowns: barotropic velocity at the reference level needed in thermal wind integration and vertical eddy diffusion coefficients between the vertical layers into which the box is divided.

The solution to this set of equations is sought with the total inversion algorithm of Tarantola and Valette (1982) (Mercier, 1986). In this algorithm, the budget property equations are used as constraints and are combined with *a priori* values for the unknowns in a cost function; the cost function is weighted with *a priori* errors of the constraints and unknowns. Minimization of the cost function provides new (after inversion) values for the unknowns and for their associated errors. The algorithm is flexible enough to handle additional constraints, simply including them in the cost function. Therefore, the unknowns of the inverse model are: the reference level velocity (u_r), normal to the hydrographic lines, for all 69 station pairs; and the vertical diffusivity (K_v) at the interface of the six layers into which we divided the box vertically. The latter are necessary to compute the diffusive fluxes in the tracer constraints that are written as a balance between advection and vertical diffusion. The limits for the six layers (Fig. 2a) were selected, according to Slater (2003), Álvarez et al. (2005) and Carracedo et al. (2014), as: 41.430 (~2500 m) to 41.455 (~2800 m), 41.455–41.475 (~3000 m), 41.475–41.490 (~3200 m), 41.490–41.505 (~3550 m), 41.505–41.515 (~3900 m) and 41.515 to bottom.

All the computed transports are considered to be positive when entering the box and include Ekman transport, calculated separately from QuikScat winds (average for July–August 2009) and distributed equally over the first 30 m.

Model constraints

The inverse model was designed to minimize a cost function and estimate u_r and K_v that better fulfil several constraints, while taking into account their respective *a priori* errors as weights in the cost function. Initially, we defined an inverse model configuration with the conservation of properties (volume, salt and heat) as general constraints and five additional volume constraints.

(a) Conservation of properties' constraints

The model was set to conserve volume and salt from surface to bottom along the three sections (Table 1a), which forces the flow through the box sections to compensate for:

- (i) the evaporation minus precipitation minus river runoff ($E - P - R$) balance in CAIBOX (0.040 Sv), plus the $E - P - R$ balance in the Mediterranean Sea (0.051 Sv), both estimated from ERA40 summer data. Thus, 0.091 ± 1 Sv enters the box in the three sections. Note that the 1 Sv uncertainty approximately accounts for the contributions to the volume balance of the errors (assumed uncorrelated) in the Ekman transport (0.4 Sv, estimated as the root mean squared value

for the summer months), the volume transport over the continental shelf (0.5 Sv, estimated from Haynes and Barton, 1990; and Mazé et al., 1997), the bottom triangles and high frequency variability in the density field (0.8 Sv, adapted from Ganachaud, 2003, who suggested 1–2 Sv for a transatlantic section) and the estimate of the $E - P - R$ (0.007 Sv, taken as the root mean squared value for the summer months). Previous $E - P - R$ estimates for similar boxes are those of Slater (2003), who gave values of 0.076 and 0.061 Sv for 1988 and 1998 (computed from global air–sea heat and momentum from the Southampton Oceanography Centre, Josey et al., 1998) and Álvarez et al. (2005), who estimated the $E - P - R$ flux as 0.086 Sv. After inversion, from the residual of that constraint, the value we actually obtained was 0.125 ± 0.67 Sv, slightly higher than our prediction but in agreement in the range of uncertainty. We included the $E - P - R$ term in the Mediterranean Sea because there is no eastern section closing the box at the Gibraltar Strait.

- (ii) a null net salt flux across the Gibraltar Strait, which implies net transport across the limits of the box ($0 \pm 36.2 (\times 10^9)$ Sv pu), as we assumed a steady salt content in the box.

As general constraints, in accordance with Slater (2003), Álvarez et al. (2005) and Carracedo et al. (2014), volume, salt and heat were conserved independently in the six previously defined density deep layers. The uncertainties in these deep layers, not in contact with the atmosphere, were taken to be equal to the *a priori* diffusive transports of tracer across the top of each layer, computed from the *a priori* values of K_v (see Section 'Reference levels and *a priori* u_r and K_v values and uncertainties). Overall, the uncertainties obtained were 0.2 Sv for volume, $0.01 (\times 10^9)$ kg s^{-1} for salt and 0.01 to 0.06 ($\times 10^{13}$) W for heat.

(b) Additional constraints

Additional constraints were used in the northern section and in close-to-coast areas (Table 1), following a model configuration equivalent to that used with climatological data (Carracedo et al., 2014). Most (i to iii) are fluxes at locations at which the variation around the mean flow appears to be well estimated, allowing a constraint to be written; the last (iv) includes the water mass conservation for the Labrador Sea Water (LSW). These additional constraints to the model weight the solution towards well-documented circulation patterns. The constraints are:

- (i) In accordance with Lherminier et al. (2010), -0.8 ± 0.8 Sv was imposed in the north section (station pairs 1–24) from $\sigma_4 = 45.85$ kg m^{-3} (σ_n , potential density of [1000 + value] kg m^{-3} referred to $n \times 1000$ db) to bottom, in agreement with the estimate of McCartney et al. (1991) of 0.83 Sv for waters with $\theta < 2.05$ °C at 36°N between 16 and 19°W. This accounts for the northward flow of North-East Atlantic Deep Water (NEADW) in the Iberian Basin (Fig. 1).
- (ii) For the eastern boundary of the north section (station pairs 1–11), -1 ± 2 Sv from $\sigma_2 = 36.94$ kg m^{-3} to bottom was set, according to Lherminier et al. (2010).
- (iii) In the southern section (in the Lanzarote passage, station pairs 64–69) we used two climatological “summer” transports derived from 9 years of direct estimates (Fraile-Nuez et al., 2010): -0.57 ± 1.13 Sv between surface and $\gamma = 27.3$ kg m^{-3} (γ , neutral density of [1000 + value] kg m^{-3} ; Jackett and McDougall, 1997), accounting for Eastern North Atlantic Central Water transports and 0.44 ± 0.37 Sv, between $\gamma = 27.3$ and 27.7 kg m^{-3} , for influenced Antarctic Intermediate Water (AA).

Table 1Volume, salt and heat constraints in the inverse model. Positive transport enters the box. The term T_D refers to the *a priori* vertical diffusive transport.

Constraint	Value	Horizontal/vertical domain	After inversion
Surface-to-bottom volume conservation (Sv)	0.091 ± 1	Whole box/whole water column	0.125 ± 0.67
Surface-to-bottom salt conservation ($\times 10^9 \text{ kg s}^{-1}$)	0 ± 36.2	Whole box/whole water column	2.4 ± 25
Volume, salt and heat conservation by six deep layers (Fig. 2a)	$0 \pm T_D$	Whole box/ $\sigma_3 > 41.430 \text{ kg m}^{-3}$ ($\sim 2600 \text{ m}$ to bottom)	-0.07 to 0.12
Surface-to-bottom LSW conservation (Sv)	0 ± 0.3	Whole box/see water mass distribution, Fig. 7	-0.08 ± 0.26
(1) NEADW _L –Iberian Basin transport (Lherminier et al., 2010) (Sv)	-0.8 ± 0.8	North section (station pairs 1–24)/ $\sigma_4 > 45.85 \text{ kg m}^{-3}$ ($\sim 3700 \text{ m}$ to bottom)	-0.72 ± 0.8
(2) Eastern boundary current (Lherminier et al., 2010) (Sv)	-1 ± 2	Eastern Boundary Current (station pairs 1–11)/ $\sigma_2 > 36.94 \text{ kg m}^{-3}$ ($\sim 2000 \text{ m}$ to bottom)	-0.25 ± 2
(3) Central water Lanzarote Passage transport (Fraile-Nuez et al., 2010) (Sv)	-0.57 ± 1.13	Lanzarote Passage (station pairs 64–69)/surface to $\gamma = 27.3 \text{ kg m}^{-3}$ (0–600 m)	-1 ± 1.13
(4) AA Lanzarote Passage transport (Fraile-Nuez et al., 2010) (Sv)	0.44 ± 0.37	Lanzarote Passage (station pairs 64–69)/ $\gamma = 27.3$ to $\gamma = 27.7 \text{ kg m}^{-3}$ (600–1100 m)	0.46 ± 0.37

AA, diluted form of Antarctic Intermediate Water; NEADW_L, North-East Atlantic Deep Water Lower.

(iv) The idea of deep water mass conservation was reinforced by adding a new constraint involving an eOMP solution (Álvarez et al., 2005; Pardo et al., 2012; Carracedo et al., 2014). In this case, the inverse model was constrained to conserve LSW in the whole box.

Optimum multiparametric analyzes (Tomczak, 1981a,b) are mathematical approaches based on real data for studying diapycnal or isopycnal mixing of water masses in a certain region. The main principle is that physical or chemical properties measured at each point are considered to be the result of the mixing of a certain number of source water masses, which must have well-known physical and chemical characteristics. Carracedo et al. (2012) described source water mass characterization in detail. The outcome of the analyzes is the contribution (x_i) of each source water mass to the mixing process. The main model assumptions are: (1) Mixing between source water masses is linear. (2) The observed properties are assumed to be conservative (θ and S , even SiO_4), or a biogeochemical term (ΔO_2) is added to account for non-conservative tracers (NO_3 , PO_4 and O_2) through predefined stoichiometric coefficients ($r_{\text{O/N}} = 9.3$, Pérez et al., 2001; and $r_{\text{O/P}} = 163$, Anderson and Sarmiento, 1994). (3) The source water mass properties are accurately known (within their standard deviation). (4) The mass balance equation must be satisfied at any point. (5) The mixing contribution of each source water mass is always positive.

The obtained x_i values are in the range 0–1 and refer to the amount of a certain source water mass, i , implicated in the mixing processes. Their contributions (x_i) can be used as a tracer to obtain water mass transport simply by multiplying the contribution and volume transport fields. Additional constraints can be included in the inverse model to fit specific well-known water mass transport better in the whole box or in determined areas. As water mass limits are based not only on definitions of density layers but also on thermohaline and chemical tracers, this water mass-specific constraint closely defines the LSW limits. In order to be consistent with the volume errors by layers, an uncertainty of $\pm 0.3 \text{ Sv}$ was established.

Reference levels and *a priori* u_r and K_v values and uncertainties

The reference levels for geostrophic computations (Fig. 2) were selected *a priori* after studying both the vertical shears of the geostrophic velocities and the water mass fields. As the reference level defines where the *a priori* values and uncertainties for u_r are taken, we mainly searched for reference levels with zero or close to zero velocities, although finally we used velocities that were not negligible.

A reference level must ensure that *a priori* water mass transport (geostrophic transport in this case) is compatible with water mass

spreading directions, according to the literature. Previous similar studies in the Iberian Basin (Saunders, 1982; mcartney, 1992; Arhan et al., 1994; Álvarez et al., 2002, 2005; Lherminier et al., 2007, 2010; Álvarez and Álvarez-Salgado, 2009) used $\sigma_3 = 41.49 \text{ kg m}^{-3}$ ($\sim 3200 \text{ dbar}$), or bottom if shallower, as the reference level. Our choice joins this σ_3 level with a shallower one at $\gamma = 27.922 \text{ kg m}^{-3}$ as the interface between intermediate and deep waters (Machín et al., 2006) for station pairs 55–65 (southern section). Machín et al. (2006) based their choice on the work of Dickson et al. (1985) and on direct velocity estimates close to the Canary Basin area given by Müller and Siedler (1992), which were $0.01\text{--}0.02 \text{ m s}^{-1}$ in deep-bottom waters, slightly higher than those found in the Iberian Basin (up to $\sim 0.01 \text{ m s}^{-1}$). Additionally to incorporation of this shallower reference level, SADC data were used to give a closely defined level of known motion (at $\sim 400 \text{ dbar}$) off the African coast (between station pairs 65–69 in the Lanzarote Passage, Fig. 1)

The *a priori* associated uncertainty for velocities at the reference level was established at 0.02 m s^{-1} for all station pairs except for those shallower than 2000 dbar , for which we used 0.03 m s^{-1} . These values are compatible with those given by Machín et al. (2006), on the basis of eddy kinetic energy (velocity variance), for an enclosed box in a similar area (0.02 m s^{-1} for the reference level at $\gamma = 27.38 \text{ kg m}^{-3}$ and $0.012\text{--}0.016 \text{ m s}^{-1}$ for a deeper one, $\gamma = 27.38\text{--}28.07 \text{ kg m}^{-3}$). They result in clear after-inversion-normalized velocities at the reference level (ratio of after-inversion u_r minus prior-inversion u_{r0} uncertainty to prior u_r uncertainty ~ 0.5). The velocities at the reference level (and its error), before and after inversion, are shown in Fig. 3.

The last step in applying the inverse model is to choose the correct values for the vertical diffusivity term K_v . This was set *a priori* to a general value of $10^{-4} \pm 10^{-4} \text{ m}^2 \text{ s}^{-1}$ for all the interfaces between layers (Mazé et al., 1997; Polzin et al., 1997; Lux et al., 2001). The values after inversion ranged between 0.9 and $1 (\times 10^{-4}) \text{ m}^2 \text{ s}^{-1}$.

Model solution

The unknown velocities at the reference level were obtained by minimizing the weighted sum of the squared residual of the property budget conservation constraints, the squared departures from *a priori* values of the reference-level velocities and the squared residuals of additional transport constraints. As the weight of each constraint is inversely proportional to its uncertainty, constraints with large uncertainties provide less information than those with small uncertainties. A total of 75 unknowns (69 u_r station pairs and 6 K_v) and 28 constraints made up the system. Fig. 3 shows the resulting absolute velocity field.

We then compared the velocities from our inverse model solution with SADC data velocities (Fig. 4). Departing from SADC zonal

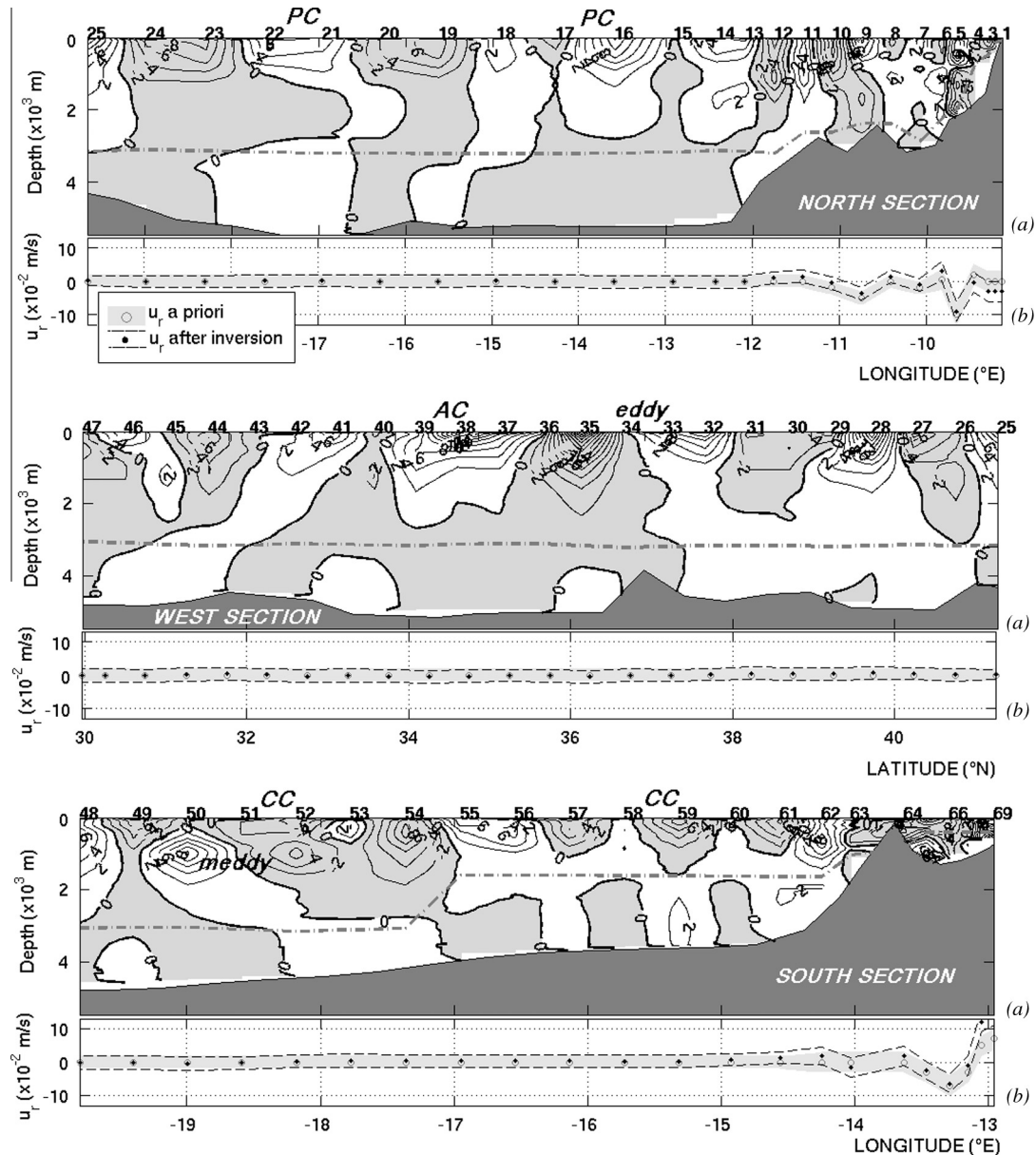


Fig. 3. (a) Absolute geostrophic velocities ($\times 10^{-2} \text{ m s}^{-1}$) by section. Grey shaded (white) areas are negative-outflowing (positive-inflowing) velocities. Dashed dark grey line corresponds to the reference level. (b) Velocity at the reference level before (grey circles, with grey shaded area corresponding to the error before inversion, i.e., $2 \cdot 10^{-2} \text{ m s}^{-1}$) and after inversion (black dots, with dashed lines corresponding to the error after inversion). PC, Portugal Current; AC, Azores Current; ACC, Azores Counter-Current; CC, Canary Current.

and meridional components, orthogonal velocities to the box sections were computed and then averaged among stations for the ~ 100 – 450 -dbar layer (or, in shallower stations, to the maximum possible depth). This vertical range avoids the Ekman layer and the deepest SADCPC, which have noisy records. When gaps appeared in the SADCPC register (station pairs 10–12, 35–37 and 40), due to technical problems in recording, Aviso altimetry-derived geostrophic velocities were used instead (Gourcuff et al., 2011) (see estimated mean Aviso velocity normal to the section by station pairs in Fig. 4). In the northern and western sections, SADCPC and Aviso velocities were more concordant (with a correlation $>60\%$, not shown) than in the south section.

SADCPC data can be included in the model as additional constraints (Lherminier et al., 2007, 2010), in an attempt to find a better solution for the inverse problem (Mercier, 1986). Nevertheless, this is true only when these new constraints provide useful infor-

mation for the solution, i.e. when their inclusion in the inverse problem gives sounder after-inversion results, because the solution has been forced to fulfil the new constraints. Conversely, if the inverse model without SADCPC constraints is able, within the range of uncertainty, to provide results compatible with the SADCPC transports, as in this case (Fig. 4), it is wiser not to include them in the inversion but to use them for external validation of the inverse model results. Fig. 4 shows that the after-inversion and SADCPC velocities are similar and show the same pattern for the 100–450-dbar pressure range ($\text{rms}(u_r \text{ inverse model}) = 0.53 \cdot 10^{-2} \text{ m s}^{-1}$, $\text{rms}(u_r \text{ SADCPC}) = 0.54 \cdot 10^{-2} \text{ m s}^{-1}$).

As shown in Table 2, the residuals of conservation constraints are lower than the *a priori* error. As we were looking for a better volume-, heat- and salt-balanced solution at the expense of an *in situ* absolute-velocity weighted solution, the discussion is based on the inverse model solution.

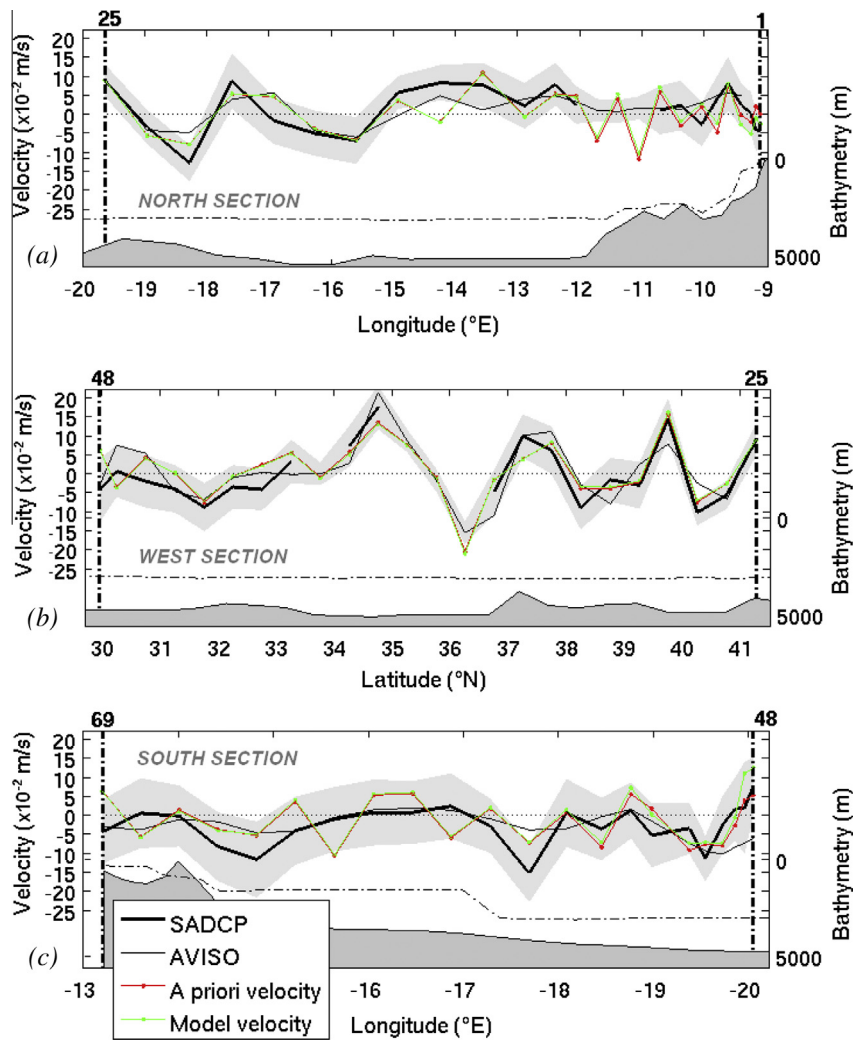


Fig. 4. Mean velocity by station pair (normal to the sections, positive entering the box) for the layer 100–450 dbar (a, north; b, west; c, south). The thick black line corresponds to SADCp velocity and the thin black line to Aviso data. As Aviso data are satellite-derived, they do not correspond to 100–450 dbar but to the surface. The red line is the geostrophic velocity before inversion, while the green line is the velocity after inversion. Grey shading represents twice the standard deviation computed for each SADCp station pair velocity or the generic uncertainty for Aviso velocities (0.03 m s^{-1} ; Gourcuff et al., 2011) when SADCp data are missing (station pairs 10–13, 35–37 and 40). The numbers above the lines correspond to station pairs. (For interpretation of the references to colour in this figure legend, the reader is referred to the web version of this article.)

Results and discussion

The subtropical north-eastern Atlantic region is well characterized from a thermohaline point of view by a marked contrast between the upper and intermediate layers (0–500 and 500–2000 dbar, respectively) in the northern and southern domains

Table 2

Residuals of the model constraints after inversion. The constraints are categorized into eight classes; if one class comprises more than one constraint, the mean residual is given. The same was done for error, but in this case the root mean square is given.

Constraint	A priori uncertainty	Model residual
Surface-to-bottom volume conservation (Sv)	1	0.034
Surface-to-bottom salt conservation (kg^{-1})	36.2×10^9	2.3×10^9
Volume conservation by six deep layers (Sv)	0.08	0.03
Salt conservation by six deep layers (kg^{-1})	0.003	0.001
Heat conservation by six deep layers (PW, petawatt)	0.16	0.04
Surface-to-bottom Labrador Sea Water conservation (Sv)	0.3	0.08
Additional constraints (1–4) (Sv)	1.2	0.08

(Fig. 2a). In the upper layer, colder ($13.3 \text{ }^\circ\text{C}$) and fresher (35.77 psu) waters are located in the north (Northern Hemisphere subpolar origin), while warmer ($15.9 \text{ }^\circ\text{C}$) and saltier (36.23 psu) waters are located in the south (subtropical origin). At intermediate levels, however, colder ($7.44 \text{ }^\circ\text{C}$) and fresher (35.41 psu) waters are located in the south (Southern Hemisphere subpolar origin), while warmer ($8.2 \text{ }^\circ\text{C}$) and saltier (35.61 psu) waters appear in the north (Mediterranean origin). This pattern gives the region specific dynamics and water mass transformation. To place the discussion in a climatological framework, we compare the quasi-synoptic results of the CAIBOX summer oceanographic cruise with transport derived from the *World Ocean Atlas 2009* (WOA09; Boyer et al., 2009) in the region. The WOA09 analyzes were performed by Carracedo et al. (2014) with a similar inverse model and constraints suitable for climatological data. In the following subsections, the water column is divided according to Álvarez et al. (2005) into upper (0–500 dbar), intermediate (500–2000 dbar) and deep (>2000 dbar) layers. We describe circulation in these three main layers and also transport in the most important surface and subsurface currents in the Eastern Subtropical Gyre: the AC, the Azores Counter-Current (ACC), the PC and the CC.

Horizontal circulation

Mesoscale activity

The inferred horizontal circulation in quasi-synoptic cruises is always affected to a greater or lesser extent, depending on the survey area, by mesoscale activity. Two images of sea-level anomaly (Aviso, $1/3^\circ$ resolution) on the first and last days of the cruise (25 July 2009 and 14 August 2009, respectively) are shown in Fig. 5, giving an idea of the eddy variation during the study. The most outstanding superficial mesoscale feature that crossed the section during the cruise was an eddy located north of the AC, above 36°N (Carracedo et al., 2012). The velocity of this rotating feature was of the same order as the AC. Fig. 5c shows the temporal evolution of superficial velocities normal to the section a few days before and after the period of the cruise. The eddy took more than 2 weeks to cross the west section westwards (~ 45 km in about 18 days), which is in the range of the mean propagation speed given by Alves et al. (2002) for this kind of structure at similar locations (1.5 – 2.6 km day $^{-1}$ at 18 – 30°W , 27 – 37°N). The cruise coincided with a period of “slower” coastal currents than preceding and subsequent days, on the coasts of both Portugal and Africa.

Apart from these superficial mesoscale structures (registered by Aviso images), at intermediate level one meddy crossed the south section, centred at 1000 dbar (Fig. 3c, station pairs 50–52). A meddy (McDowell and Rossby, 1978) is an anticyclonic rotating lens of warm, salty Mediterranean Water (MW) with typical azimuthal velocities up to 3 m s $^{-1}$ (Armi and Zenk, 1984; Richardson et al., 2000) and an internal structure dividing the “core” from the “outside” at a radius of 10 – 40 km. This boundary is typically characterized by a steep change in hydrological properties (Paillet et al., 2002). In our case, the core of the meddy (salinity and temperature maximum) was sampled only at station 53 (Fig. 2b, southern section); therefore, its diameter was <80 km. Asymmetry has been found between the negative and positive lobes of this meddy, which are probably related to interaction with larger advecting velocities (Carton et al., 2010). This asymmetry leads to a net positive inflow of 0.6 Sv (21.9 Sv psu). In addition, we found a maximum meddy velocity of 1 m s $^{-1}$, lower than the value reported in the literature, raising the question of whether it was sampled at its centre. Three weeks or less thus appears to be long enough for some eddies and rotating features to displace or migrate (Fig. 5). Caution is therefore required with regard to the synoptic assumption. The inverse model must be set up correctly in order to account for these sources of geostrophy bias, by establishing reasonable prior uncertainties for the constraints.

Volume transport

Four main surface or subsurface currents were identified in the easternmost part of the Atlantic Subtropical Gyre (Fig. 3) and their net volume transport computed. AC crosses the west section (20°W) between 34.3 and 35.7°N , with a transport of 13.1 ± 2.5 Sv. This value is comparable (within the error) to that estimated by Carracedo et al. (2012) for the same cruise from thermal wind equations referenced to 2000 dbar (11.2 Sv). Paillet and Mercier (1997) solved an inverse model with a set of hydrographic data gathered during spring–summer between 1981 and 1991 and obtained a mean AC transport of 10 – 12 Sv. Our results match their estimates reasonably well and are consistent with values in the literature for this current at similar longitudes: 9 – 12 Sv between 30 and 40°W (New et al., 2001), 6.8 – 7 Sv at 21 – 19°W (Alves et al., 2002) and 13.9 Sv at 24.5°W (Comas-Rodríguez et al., 2011), the latter obtained during a cruise in the same year as CAIBOX but in a different season (October–November).

North of the AC, between 37.74 and 39.24°N , we identified the westward flow centred at ~ 600 dbar, known as the ACC (Onken, 1993; Paillet and Mercier, 1997; Alves et al., 2002; Pérez et al.,

2003; Kida et al., 2008). The presence of a surface anticyclonic eddy between the AC and ACC currents, described in the previous section, shifted the ACC further north than expected (Carracedo et al., 2012). The warm temperature of the eddy core suggested that it originated from meandering of the AC (pinching-off phase, Alves et al., 2002). Dynamically, this eddy enhances the AC–ACC system and, in this particular case, contributes with a westward net flow of -8.8 ± 3.8 Sv. Without the eddy influence, ACC transport is -5.2 ± 2.1 Sv (Table 3), which leads to an AC:ACC ratio of 2.5 (Carracedo et al., 2014).

The net flow south of the AC (southwest corner of the box and south section) between the surface and 600 m has been attributed to the CC, with a transport of 7.1 ± 1.1 Sv. If we consider that the AC is the source of the CC (Pérez-Hernández et al., 2013), $\sim 54\%$ of the AC recirculates south–southwest to take part in the CC. There is, however, controversy about the continuity of the AC–CC. While hydrography-based inverse model studies (Paillet and Mercier, 1997; Hernández-Guerra et al., 2005; Machín et al., 2006; Pérez-Hernández et al., 2013; Carracedo et al., 2014) point to clear continuity, numerical models do not provide complete support (Pérez et al., 2007; Mason et al., 2011). By reproducing the seasonal variation in the CC in a high-resolution numerical model, Mason et al. (2011) concluded that it was relatively insensitive to upstream variation from the AC and attributed seasonal modulation in the CC to the two large-scale, coherent, anomalous structures that propagate westward from their origin near the African coast.

With this issue in mind, but lending weight to inverse model results, we assume that the CC is fed by the AC. The remaining AC continues to the Gibraltar Strait, some of it recirculating northwards (Barton, 2001), but it is also fed from the north (Paillet and Mercier, 1997) so that it does not weaken eastwards. Kida et al. (2008) used a numerical model that lacked the wind-driven gyre representation to study the mechanism by which the Mediterranean overflow might drive the AC. They calculated that 4 Sv of AC reached the Gulf of Cadiz region (see their Fig. 3), part of it entraining into the MW layer (<2 Sv) and <1 Sv arriving, ultimately, in the Gibraltar Strait.

The 7.1 ± 1.1 Sv estimated for the CC transport agrees with the WOA09 spring–summer estimate of 6.0 ± 0.4 Sv (Carracedo et al., 2014) and those of other authors (6 Sv, Paillet and Mercier, 1997; 5.8 ± 0.6 Sv in September 2003, Hernández-Guerra et al., 2005; 4.8 Sv in June–July 1998, Machín et al., 2006; 6.2 ± 0.6 Sv in October–November 2009, Pérez-Hernández et al., 2013). The CC is known to be stronger in summer near the African coast, east of the Canary Islands (Navarro-Pérez and Barton, 2001; Machín et al., 2006; Arístegui et al., 2009). Machín et al. (2006) reported a net summer transport between islands of -4 ± 0.8 Sv (surface to $\gamma = 27.38$ kg m $^{-3}$, roughly 700 dbar), comparable to our finding (-4.5 ± 1.3 Sv). The increased off-shore CC transport in CAIBOX with regard to the summer 1998 cruise (Machín et al., 2006) is in agreement with the detected strengthening of the subtropical gyre above the thermocline between early 2009 and mid-2010, balanced by a decrease in the southward flow of NEADW_L below 3000 m, that is, a down-turn of the Atlantic meridional overturning circulation (McCarthy et al., 2012; Smeed et al., 2013), as also pointed out by Pérez-Hernández et al. (2013).

Net transport across the northern section of the PC was quantified for 18°W onshore and between the surface and 800 m. We obtained a value of 4.5 ± 1.4 Sv, in good agreement with that of Paillet and Mercier (1997), who estimated a total of 8 Sv recirculating from the North Atlantic Current southwards in the eastern basin (~ 4 Sv east of 20°W).

The main circulation features intersected by CAIBOX can also be identified from the barotropic stream functions, which were computed by accumulating surface, intermediate, deep and

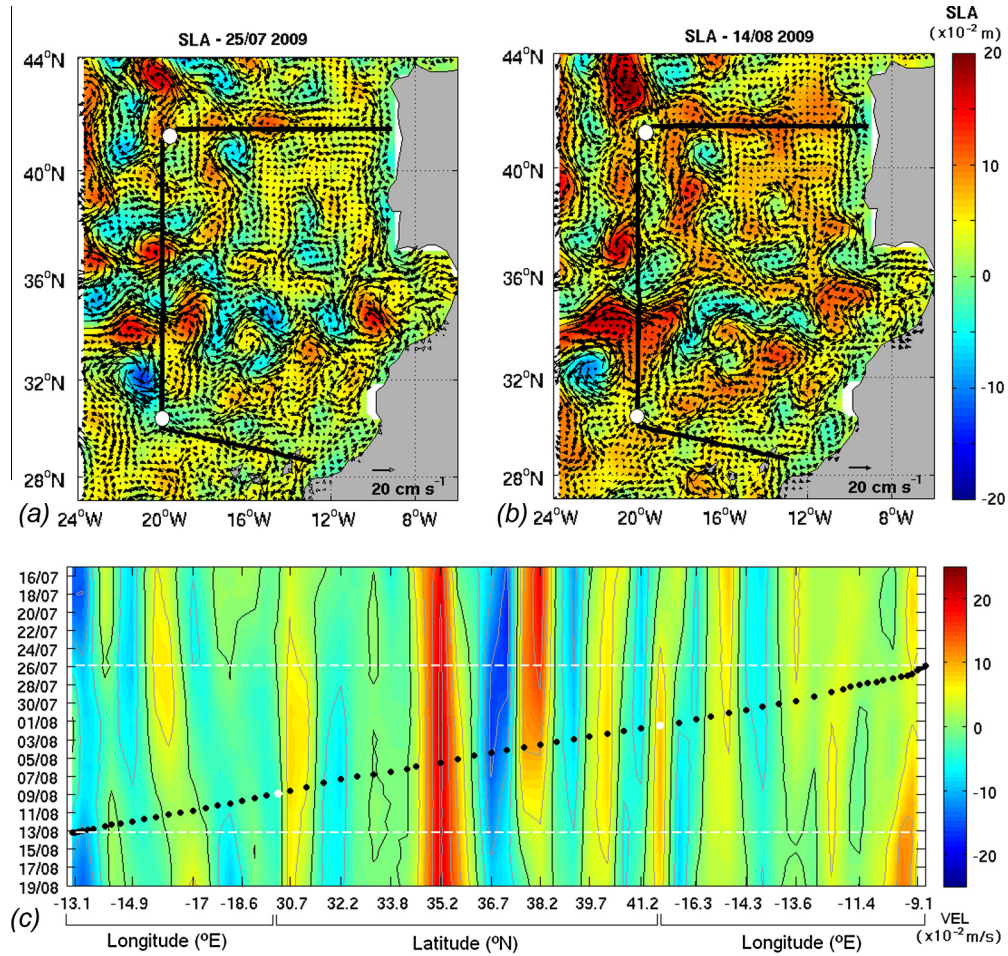


Fig. 5. Sea level anomaly (SLA; $\times 10^{-2}$ m) for (a) first and (b) last days of the cruise. Black straight line represents the cruise track. White dots indicate the corners of the box (station pairs 25 and 47). (c) Hovmöller diagram of geostrophic (altimetry-derived) velocities ($\times 10^{-2}$ m s^{-1}) for the period of study (inside-box view, from station pair 1, off Portugal coast, to station pair 69, off African coast). Black dots represent the station pair positions. Thin white-dashed lines mark the beginning and ending dates of the cruise. White dots indicate the corners of the box (station pairs 25 and 47). Note the lack of velocity data for the first three station pairs.

Table 3

(a) Spatial limits defining main surface and subsurface system currents; (b) volume (Sv), salt (Sv psu) and heat (PW) transport of each current and comparison with summer WOA09 climatology. PC, Portugal Current; PCC, Portugal counter-current; ACC, Azores Counter-Current; AC, Azores Current; CC, Canary Current.

Current	Station pairs		Horizontal limits		Vertical limits (dbar)	
(a)						
PC	1–26		9.1–20°W		0–800	
PCC	1–26		9.1–10.4°W		0–300	
ACC	34–36		36.7–35.7°N		0–1600	
AC	36–39		35.7–34.3°N		0–1600	
CC	43–69		20–12.9°W		0–600	
	Net transport (Sv)		Net salt transport (Sv psu)		Net heat transport (PW)	
	Summer WOA09	CAIBOX	Summer WOA09	CAIBOX	Summer WOA09	CAIBOX
(b)						
PC	1.5 ± 0.4	4.5 ± 1.4	52 ± 15	160 ± 51	0.08 ± 0.02	0.23 ± 0.07
PCC	–0.004 ± 0.001	–0.3 ± 1.8	–11 ± 2	–1.2 ± 6	–0.02 ± 0.004	–0.002 ± 0.01
ACC	–1.9 ± 0.7	–5.2 ± 2.1	–67 ± 25	–188 ± 75	–0.06 ± 0.02	–0.25 ± 0.1
AC	6.8 ± 0.9	13.1 ± 2.5	247 ± 31	470 ± 88	0.41 ± 0.05	0.70 ± 0.1
CC	–5.3 ± 0.4	–7.1 ± 1.1	–192 ± 15	–256 ± 50	–0.34 ± 0.03	–0.46 ± 0.08

top-to-bottom integrated transport from Africa to the Iberian Peninsula. The summer climatology results of WOA09 and the results of CAIBOX are plotted together for comparison in Fig. 6. The upper horizontal circulation (Fig. 6a) shows the well-known upper anticyclonic circulation in the North Atlantic Subtropical Gyre, with water mainly inflowing through the west section and outflowing southwards. The circulation patterns are close to those estimated

by WOA09, although mesoscale variation is obvious in the CAIBOX results for the upper and intermediate layers. The smoothed character of the climatological data indicates widened currents, i.e. shallower slopes in the accumulated horizontal transport. In the CAIBOX results, the steep slopes define clearer (and narrower) spatial limits for the main currents (CC, 0–900 km from Africa; AC, 1100–1250 km; ACC, 1600–1700 km; PC, 2300 km to the Portu-

guese coast). The greatest difference from the climatological mean appears in the west section at the location of the AC–ACC system, because the AC is a highly meandering current, dominated by strong geostrophic turbulence (Alves et al., 2002).

The main differences in the vertically integrated transport profiles (Fig. 6b) are in the intermediate layer, in the west and south sections, where transport was higher in the CAIBOX results, with higher outflow through the west section and higher inflow through the southern one. The deep circulation is characterized by weaker flows than those at the intermediate and upper levels (Fig. 6a, third panel), which are known to be strongly constrained by topography. The cumulative transport in the CAIBOX results and the mean of the WOA09 results are similar in this layer. In the Canary basin, across the south section, there is a deep (weak) cyclonic circulation

cell (Machín et al., 2006; Carracedo et al., 2014). A broader cyclonic deep circulation cell is found in the northern half of the box, with deep water entering across the north of the west section (entrance enhanced in the CAIBOX results) and flowing out across the northern section.

Heat and salt fluxes

Understanding how salinity and heat are exported and imported from and to the interior of the CAIBOX helps to clarify thermohaline circulation inside the box. The salt and heat fluxes were computed as $\iint \rho S v dx dz$ and $\iint \rho c_p \theta v dx$, respectively, where ρ is seawater density, $S = S(x,z)$ is salinity, $\theta = \theta(x,z)$ is potential temperature, $v(x,z)$ is the velocity orthogonal to the section, c_p is the specific heat capacity, x is the section coordinate, and z is

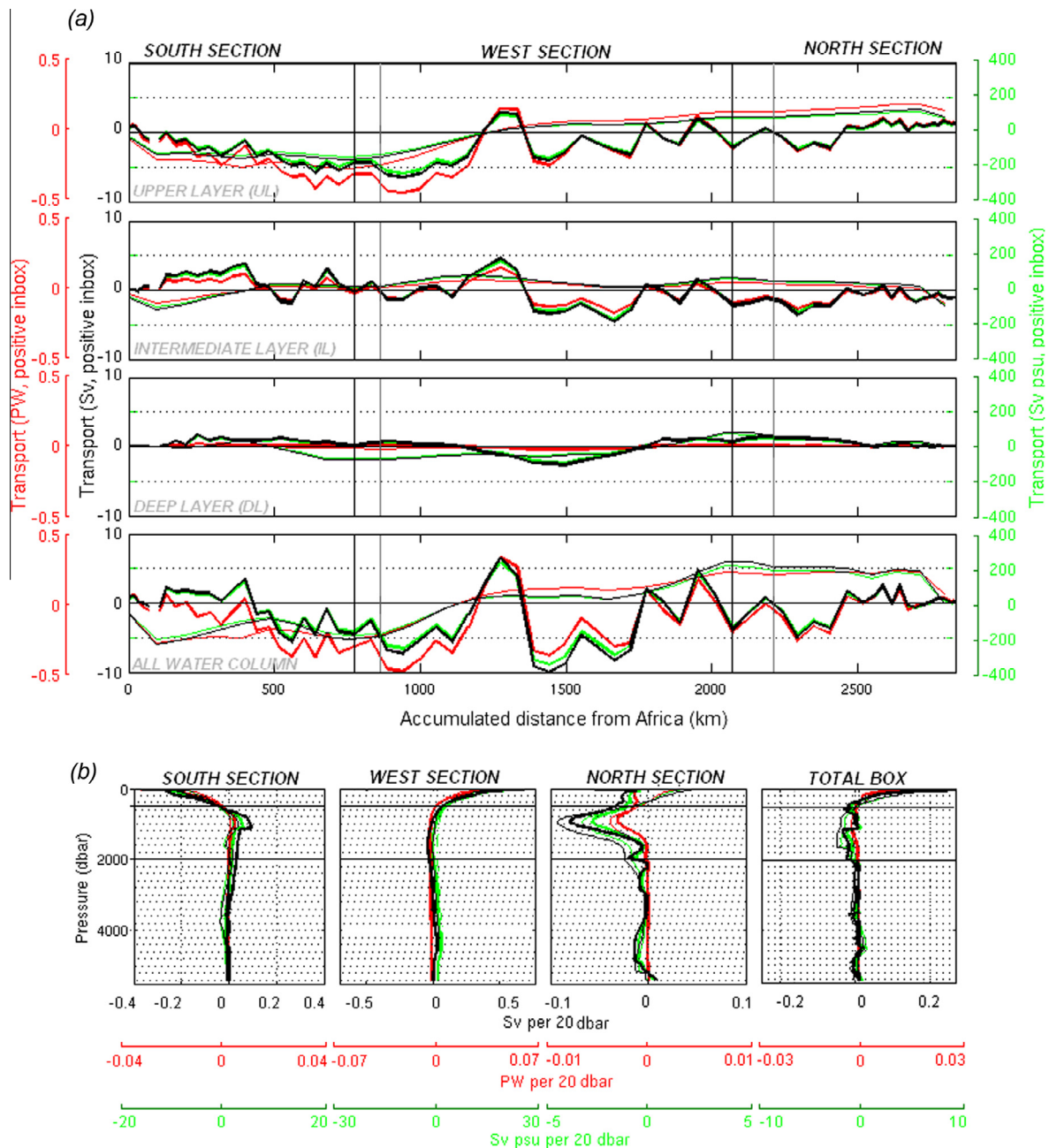


Fig. 6. (a) Horizontal accumulated (from African to Iberian Peninsula coasts) transports divided into three vertical layers (0–500 dbar, 500–2000 dbar and 2000 dbar–bottom) and for the whole water column. Black, red and green lines correspond to volume (Sv), heat (PW) and salt (Sv psu) transport, respectively. Bold lines correspond to CAIBOX, while thin lines represent WOA09 climatology results (Carracedo et al., 2014). (b) Mean vertical profiles of volume transport for the three sections and the whole box. (For interpretation of the references to colour in this figure legend, the reader is referred to the web version of this article.)

depth. The salt flux was normalized by a mean density to obtain units of Sv psu.

The constraint to conserve the total box volume (Table 2 and Section ‘Reference levels and *a priori* u_r and K_v values and uncertainties’) was not strictly fulfilled. There is, after model inversion, net transport into the box of 0.125 Sv (“effective fresh water transport”), which is physically justified by the overturning circulation typical of this region, outflowing waters being saltier than inflowing waters. We can transform this net volume transport into “effective salt transport” by multiplying by the mean box salinity for the upper 2500 dbar (35.51 psu), to obtain 4.5 Sv psu. Taking into account that the net salt flux after inversion was 2.4 Sv psu, 2.1 Sv psu would not come from the net volume imbalance but from net salt exportation. This simple calculation allows us to compare our results with those of previous studies in the same area, such as those of Álvarez et al. (2005) (2.98 ± 0.3 Sv psu) and Slater (2003) (2.5 and 2.2 Sv psu), and verify that the net balances remain comparable whatever method is used to solve the absolute velocity field.

The AC is the main source of heat (0.7 ± 0.1 PW) and salt (470 ± 88 Sv psu) into the box (Table 3b). As already pointed out, the AC recirculates into the CC, however, the proportion of heat (67%) transferred by the AC is higher than the proportion of volume ($\sim 54\%$). Fig. 6a shows how the horizontal accumulated transport of volume and heat differs in the upper layer of the box. This is because, while the AC keeps flowing eastwards and south-eastwards, its heat content increases by incoming net radiation from the atmosphere. We estimated from ERA40 a net air–sea heat transport of 0.15 PW (towards the ocean) for the whole CAIBOX superficial area. As CAIBOX is a region with a positive net $E - P - R$ term (~ 0.038 Sv), the resulting superficial central waters flowing out in the CC will be warmer and saltier than the incoming AC central waters. The PC also imports heat and salt into the box, although three times less than the AC (0.23 ± 0.07 PW and 160 ± 51 Sv psu, respectively). This is expected, because PC transport is twice as low as that of the AC, and the central water transported into the PC is mainly of subpolar origin, i.e. fresher and colder (Ríos et al., 1992; Pérez et al., 2001; Carracedo et al., 2014). Conversely, the main upper heat and salt-box exporting paths are the CC (-0.46 ± 0.08 PW and -256 ± 50 Sv psu) and the ACC (-0.25 ± 0.1 PW and -188 ± 75 Sv psu). Because of weak circulation below 2000 dbar, the salt flux barely exceeds 100 Sv psu, and heat transport is virtually absent. The deep waters are cold enough that they do not introduce heat imbalance within the limits of the box.

Water mass budgets and fates

Fig. 7 shows the spatial distribution of the water masses in the CAIBOX section, as estimated with the eOMP, demonstrating the main advective water masses paths. Briefly, the upper layer (0–500 dbar) is occupied by the subtropical modes (southwest domain) of central waters (Madeira Mode Water, MMW; Subtropical Eastern North Atlantic Central Water, ENACW_T). “H” is the point on the θ/S diagram that delimits ENACW_T from the subpolar variety (ENACW_P) (Ríos et al., 1992) (Fig. 2b) and is situated along the interface between the upper and intermediate layers, around 500 dbar, deepening its distribution at the location of the ACC. The intermediate layer (500–2000 dbar) contains ENACW_P, MW and AA. The patchy distribution of the ENACW_P and MW cores corresponds to the velocity field, being present at those locations with inflowing and outflowing fluxes, respectively. The major contribution of MW is in the north section, off the Portugal slope. LSW is located down in the water column, at the intermediate–deep interface (~ 2000 dbar), with its main core at the northwest corner of the box. The deep layer (below 2000 dbar) is occupied mainly by NEADW_L and the remnants of Iceland–Scotland Overflow Water (ISOW).

Water mass budgets

Combined eOMP water mass percentages and inverse model-derived transport make it possible to discriminate the fluxes for each water mass in the region (Fig. 8 and Table 4). We see that central waters dominate the surface and (most of the) intermediate circulation, mainly involving the PC, AC–ACC and CC systems (Fig. 8a and b), with total contributions to heat and salt transport of 0.08 ± 0.1 PW and 56 ± 34 Sv psu (Table 4).

Central waters are the main transporters of heat and salt into the CAIBOX, while MW at intermediate level is the main exporter (-0.06 ± 0.1 PW and -54 ± 16 Sv psu). A total of 1.5 ± 0.4 Sv of MW flows out of the box in two main veins. This total exportation agrees with the amount or 1.6 ± 0.2 Sv given by Carracedo et al. (2014) for summer climatology, although is lower than that estimated by Álvarez et al. (2005), 2.7 ± 0.3 Sv. Álvarez et al. (2005) used a similar procedure to solve the velocity field and water mass contributions for a CAIBOX-like box, which makes their study comparable. A major difference between the two studies is that they formed their box not from a quasi-synoptic cruise but from three independent segments of three cruises, two in 1998 (a western one in May and a southern one in January) and a northern one in August 1997. That combination, which included sections from sea-

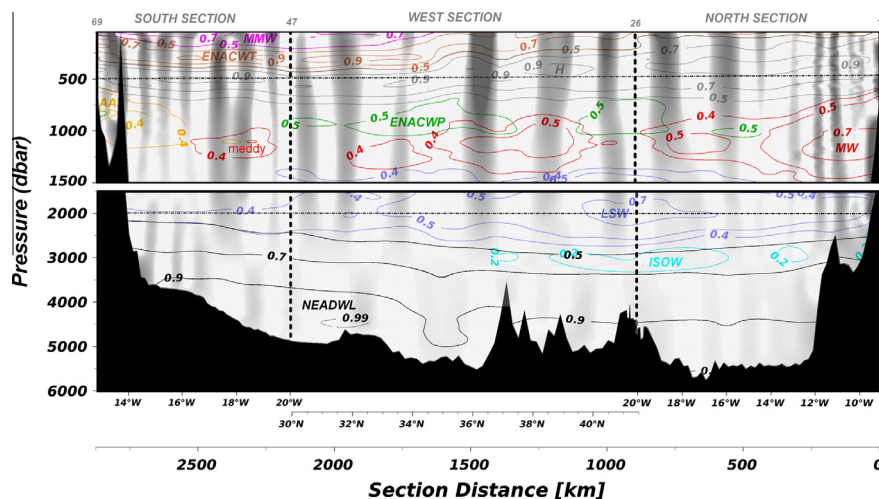


Fig. 7. Spatial distribution of water masses on the CAIBOX cruise. Contour lines are plotted for contributions >50%, except for the diluted form of Antarctic intermediate water (AA) and Mediterranean Water (MW), for which contour lines represent contributions >40%, and for Iceland–Scotland Overflow Water (ISOW), with a contribution >20%. Grey shading corresponds to negative (outflowing) geostrophic velocities. The vertical scale is amplified in the first 1500 dbar for clarity.

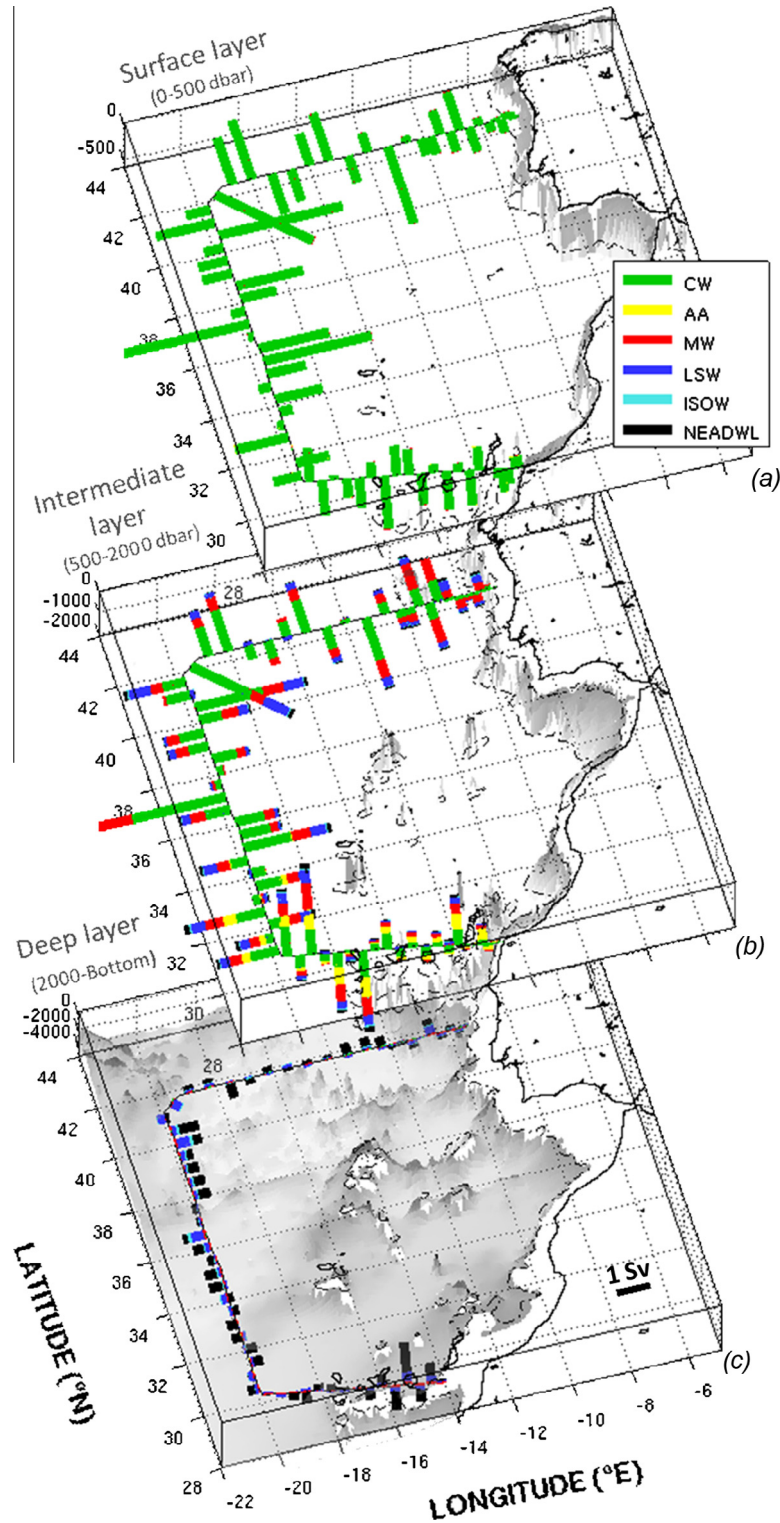


Fig. 8. Stacked bar diagrams of water mass transport (Sv) by station pairs across CAIBOX sections in (a) the upper (0–500 dbar), (b) the intermediate (500–2000 dbar) and (c) deep (2000 dbar to bottom) layers. Water masses are: Central waters (CW, sum of ENACW_T, ENACW_P and MMW), influenced Antarctic Intermediate Water (AA), Mediterranean Water (MW), Labrador Sea Water (LSW), Iceland–Scotland Overflow Water (ISOW) and North Eastern Atlantic Deep Water Lower (NEADW_L).

sons of maximum MW exportation, would have led to an overestimate of MW exportation. For the northward MW vein exportation, they obtained a value of 2.2 Sv, in contrast to our estimate of 0.95 ± 0.7 Sv. The value of 1 Sv flowing northwards given by Schmitz (1996) better supports our value. The northward vein is the main one and flows off the northern Portuguese coast, where the greatest contribution of this water mass (84%) is found

(Fig. 7) (73% in climatological summer data, Carracedo et al., 2014). The westward vein makes a maximum contribution of 62% (50% from summer climatological data). Álvarez et al. (2005) used the same thermohaline properties to characterize MW at its source region (11.74 °C, 36.5 psu), which shows the change in the contribution of MW between 1998 and 2009. They found the highest contributions of 60% and 50% in the northern and western

Table 4

Net box volume (Sv), salt (Sv psu) and heat transport (PW) by water mass and comparison with summer WOA09 climatology and [Álvarez et al. \(2005\)](#) in the same area. MMW, Madeira Mode Water; ENACW_T, Subtropical Eastern North Atlantic Central Water; ENACW_P, Subpolar Eastern North Atlantic Central Water; AA, diluted form of Antarctic Intermediate Water; MW, Mediterranean Water; LSW, Labrador Sea Water; ISOW, Iceland–Scotland Overflow Water; NEADW_L, North-East Atlantic Deep Water Lower.

Water mass	Property	CAIBOX	WOA09 Summer	Álvarez et al. (2005)
MMW	Volume	−0.61 ± 0.2		
	Salt	−23 ± 9		
	Heat	−0.05 ± 0.05		
ENACW _T	Volume	1.7 ± 0.6		
	Salt	61 ± 24		
	Heat	0.11 ± 0.1		
ENACW _P	Volume	0.5 ± 0.6		
	Salt	18 ± 21		
	Heat	0.02 ± 0.03		
Central waters	Volume	1.6 ± 1	1.9	2.50
	Salt	56 ± 34	53	88.29
	Heat	0.08 ± 0.1		
AA	Volume	0.14 ± 0.6	0.13	0.20
	Salt	5 ± 20	43	7.03
	Heat	0.002 ± 0.02		
MW	Volume	−1.48 ± 0.4	−1.62	−2.70
	Salt	−54 ± 16	−43	−97.11
	Heat	−0.06 ± 0.08		
LSW	Volume	−0.09 ± 0.4	−0.29	−0.02
	Salt	−3 ± 13	−13	−0.71
	Heat	−0.004 ± 0.04		
ISOW	Volume	−0.15 ± 0.2	0.04	0.00
	Salt	−5 ± 6	−3	0.04
	Heat	−0.002 ± 0.001		
NEADW _L	Volume	0.1 ± 0.6	−0.09	0.00
	Salt	4 ± 22	2	−0.06
	Heat	0.001 ± 0.5		
Net computed	Volume	0.13 ± 1.4	0.01	0.00
	Salt	2 ± 50	0	−2.95
	Heat	0.02 ± 0.5	0.06	0.02

sections, respectively, both of which are lower than those in 2009. [Soto-Navarro et al. \(2012\)](#) verified a positive thermohaline trend for Atlantic central waters inflowing to the Mediterranean Sea during the period 2002–2010, while no significant trend for MOW could be established. The increased contribution of MW is thus a direct reflection of the salinification of Atlantic central waters due to entrainment to the MOW level to form MW.

The difference in the MW contribution in the northern and western veins in the CAIBOX, WOA09 and [Álvarez et al. \(2005\)](#) boxes supports the idea that the MW that leaves the region through the northern vein is purer (less diluted) than that in the western vein, reinforcing the assumption that the main advection route for MW is northwards ([Danialt et al., 1994](#); [Mazé et al., 1997](#); [Paillet and Mercier, 1997](#); [Iorga and Lozier, 1999](#)). There is still controversy about whether westward MW propagation from the Cape Saint Vincent region to the west is an advective path ([Ríos et al., 1992](#)) or a meddy propagation pathway. If we accept that ACC is the main westward advective path of MW (a third part of the ACC was identified as MW by [Carracedo et al., 2014](#)), the controversy could concern the persistence of this current. The persistence of ACC is supported by recent numerical model simulations of the β -plume dynamic concept as the mechanism for formation of the AC–ACC system ([Jia, 2000](#); [Péliz et al., 2007](#); [Kida et al., 2008](#); [Volkov and Fu, 2010, 2011](#)). Although these models do not reproduce or confirm any seasonal modulation of the ACC, studies based on hydrographic data corroborate such variation: enhancement in late winter and early spring for the ACC ([Cromwell et al., 1996](#); [Carracedo et al., 2014](#)). Thus, this current could be considered a stationary westward MW advective flow. The finding that the MW core is a more diluted form of MW would indicate lack of a direct advective path from the Gulf of Cadiz, in contrast to the northward MW branch. From the total transport of MW out of the limits of our box (by whatever mechanism), we quantified

the amount of MW flowing across the northern, western and southern limits of the box and found a ratio of 65:32:3, with 65% of the total MW flowing northwards, 32% westwards and 3% southwards. This proportion is comparable to that obtained from WOA09 summer data (58:29:13) ([Carracedo et al., 2014](#)).

AA and LSW are transported mainly in the intermediate layer ([Fig. 8b](#)). The total transport of AA across the section is 0.14 ± 0.6 Sv, its presence being mainly restricted to the vicinity of the Canary Archipelago. Its major contribution (up to ~75%) is located in the Lanzarote Passage ([Fig. 7](#)), where its largest incoming transport (0.34 Sv) occurs ([Fig. 8](#)). For reference, values given in the literature for the AA transport across the Lanzarote Passage are: 0.1 ± 0.4 Sv in January 1997 to February 2001 ([Hernández-Guerra et al., 2003](#)), 0.7 ± 0.5 Sv in September 2003 ([Hernández-Guerra et al., 2005](#)), 0.3 ± 0.1 Sv in October–November 2009 ([Pérez-Hernández et al., 2013](#)), data which validate our result. Once inside the box, this water mass is likely to be (at least partially) eroded as it spreads northwards off the African coast towards the Gulf of Cadiz region ([Machín and Pelegrí, 2009](#)). At climatological scale, [Machín et al. \(2010\)](#) found an oscillating pattern for AA in this region, so that most of the northwards summer and early autumn (July–October) progression off the African coast would be returned south every late autumn (November–December), accompanied by some MW. Despite the recirculation, at annual scale, AA was found to enter the region with a net northwards flow (0.09 ± 0.57 Sv, [Fraile-Nuez et al., 2010](#); 0.2 ± 0.16 Sv, [Carracedo et al., 2014](#)). This positive summer (annual) net transport support the hypothesis that the diluted form of Antarctic Intermediate Water reaches the Gulf of Cadiz region to contribute to MW formation ([Louarn and Morin, 2011](#)).

In [Fig. 9](#), the vertical structure of the circulation (an integral view of [Fig. 8](#)) has been split up into water masses in order to quantify the thermohaline circulation, which comprises the

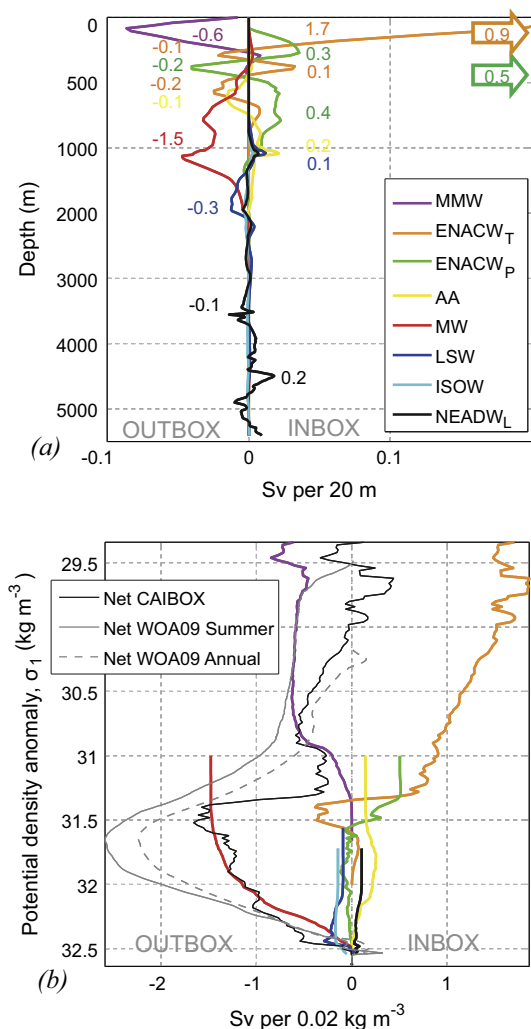


Fig. 9. (a) Vertical volume transport (Sv) profiles by water mass (integrated by depth for the whole box). (b) Vertical schematic contribution (numbers in Sverdrup (Sv), $1 \text{ Sv} = 10^6 \text{ m}^3 \text{ s}^{-1}$) by water mass (vertical scale in meters). MMW, Madeira Mode Water; ENACW_T, Subtropical Eastern North Atlantic Central Water; ENACW_P, Subpolar Eastern North Atlantic Central Water; AA, diluted form of Antarctic Intermediate Water; MW, Mediterranean Water; LSW, Labrador Sea Water; ISOW, Iceland–Scotland Overflow Water; NEADW_L, North-East Atlantic Deep Water Lower.

incoming flow of central upper-ocean waters and the return flow at intermediate levels of saltier MW. We first show the integrated Morocco–Portugal transport, by water mass, by depth (Fig. 9a) in order to differentiate the upper (~ 800 m) and lower (~ 1100 m) outflowing cores of MW. Zenk and Armi (1990) traced these two temperature and salinity maximums along the easternmost part of the Iberian Basin, the more diluted upper core mainly flowing northwards parallel to the continental shelf slope and the lower one, the purest and most voluminous, having broader horizontal extension. Nevertheless, the two cores have same θ/S properties in the eOMP model; therefore, the upper core is not an isolated maximum in the spatial distribution of the MW contribution but makes a continually decreasing contribution from its maximum lower core (Fig. 7). The net volume transport below 2800 m was quantified as $0.11 \pm 0.6 \text{ Sv}$, which is interpreted as a deep upwelling into the box, in agreement with Arhan et al. (1994) and Mazé et al. (1997) and with the original abyssal circulation model of Stommel and Arons (1960). It also agrees, within the error range, with the 0.4 Sv reported by Álvarez et al. (2005). LSW has nearly null net transport across the box ($-0.09 \pm 0.4 \text{ Sv}$), as expected because of the model constriction. In the upper layer, however,

1.4 Sv of central waters enter the box in the first ~ 400 m. Below this depth, ENACW_P and ENACW_T flow in opposite directions: ENACW_P flows out (-0.2 Sv), while ENACW_T enters the box (0.1 Sv).

Fig. 9b shows the same transport by water masses integrated from bottom to surface in density layers (σ_1). The absolute maximum of this accumulated transport corresponds to the net outflow in the lower limb of the overturning cell, which is 1.7 Sv, lower than that estimated for summer WOA09 climatology ($2.6 \pm 0.2 \text{ Sv}$, even for the annual mean, $2.2 \pm 0.2 \text{ Sv}$). The MW is the main contributor to this lower limb and is accompanied by some ENACW_T, which has already recirculated out of the box above the MW core (Álvarez et al., 2005; Carracedo et al., 2014). The upper limb is driven mainly by ENACW_T. A density range can be seen, close to the overturning maximum ($\sigma_1 = 31.5 \text{ kg m}^{-3}$), in which subtropical central water is dragged above MW out of the box (0.3 Sv).

Fates of upper and intermediate waters

Water masses inside the box not only recirculate but some are also transformed as a result of different diapycnal processes, as with central waters (MMW, ENACW_T and ENACW_P). MMW is known to be formed entirely in the box, near and to the north of Madeira Island (Fig. 10) by wintertime convection (Siedler, 1987). Spreading of MMW is limited to the north by the Azores Front, although we also found it in the eddy located north of the AC. Fig. 10 shows five regions of interest. The surface geostrophic velocity field has been superimposed to help interpretation of the fates of subtropical central waters within the box once they cross the CAIBOX sections. In this figure, we see that MMW flows out of the box into the CC system (1.34 Sv , region 5) and recirculates again into the box across the western section (0.73 Sv , region 4), resulting in anticyclonic circulation with a final net export of ($1.34 - 0.73$) $0.61 \pm 0.2 \text{ Sv}$. The circulation pattern of ENACW_P is also anticyclonic, entering the box through the northern section ($1.88 - 0.36 = 1.52 \text{ Sv}$, regions 1 and 2) and leaving the box in the AC–ACC ($-0.12 - 0.43 = -0.55 \text{ Sv}$, regions 3 and 4) and CC (-0.47 Sv , region 5) systems. This ENACW_P circulation leads to a net inflow volume transport of ($1.88 - 0.36 - 0.12 - 0.43 - 0.47$) $0.5 \pm 0.6 \text{ Sv}$. Across the northern section, 2.0 Sv of ENACW_T ($1.66 + 0.38$, regions 1 and 2) enter the box, most of which is recirculated out of the box across the western section (-1.12 Sv , region 3). The main inflow ENACW_T transport is conveyed by the AC (4.38 Sv , region 4). Although a large part of the AC–ENACW_T inflow recirculates into the CC system (3.6 Sv , region 5), leaving the box afterwards, there is a net inflow of ($4.38 - 3.6$) $0.78 \pm 0.6 \text{ Sv}$. Most of this net input ($\sim 0.6 \text{ Sv}$) will be involved in “balancing” the net MMW export, so that the remaining $\sim 0.2 \text{ Sv}$ is available to reach the Gulf of Cadiz region, together with the net northern box ENACW_T inflow ($1.88 - 1.12 = 0.54 \text{ Sv}$, which feeds the AC (regions 2 and 3), and 0.38 Sv , which directly reaches Cape St Vincent (region 1)).

The Atlantic inflow into the Mediterranean Sea (0.8 Sv , Huertas et al., 2009, 2012; Soto-Navarro et al., 2010) has two main components (Pérez et al., 2009). The Gulf of Cadiz current contributes about 40% ($\sim 0.3 \text{ Sv}$), and our estimated volume central budget indicates that the remaining $\sim 0.5 \text{ Sv}$ could be provided by ENACW_T from the offshore Atlantic current.

The above estimates (net central water transport across the limits of our box) and studies in the Gulf of Cadiz and the Gibraltar Strait indicate the probable respective contributions of central waters (ENACW_T vs. ENACW_P) to entrainment in this area of the Gulf of Cadiz. Our estimates of the contribution of each central water source to entrainment (derived from net transport in Fig. 10) are:

- 0.5 Sv of ENACW_P: the net ENACW_P incoming transport across the CAIBOX sections, which should be entirely entrained, as it does not flow across the Gibraltar Strait;

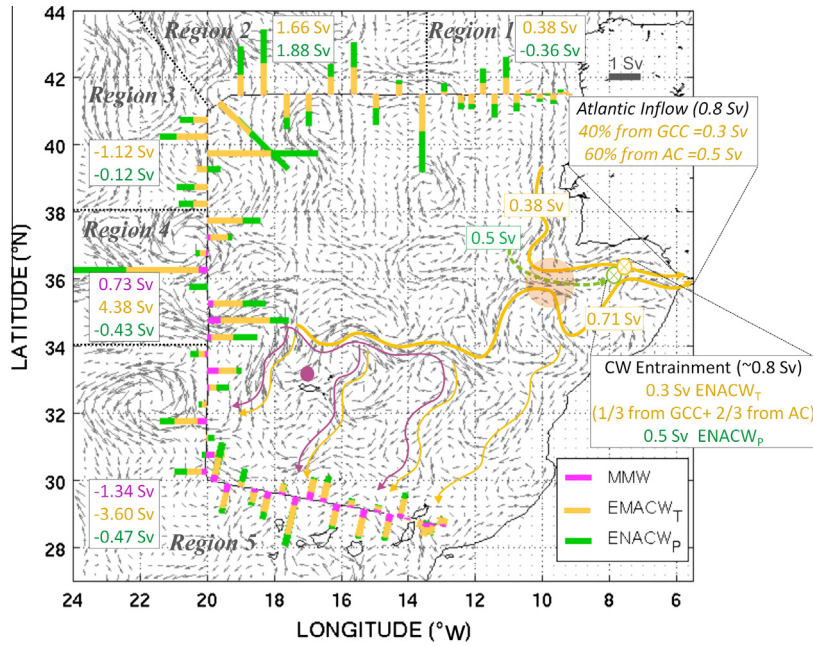


Fig. 10. Central water mass transport (Sv) computed from the inverse model by station pair across the CAIBOX section. Dotted lines separate the box into north and north-west above the Azores Current (AC), AC and south AC domains. The numbers inside boxes represent volume transport in Sv. Main recirculation paths are indicated above absolute velocity Aviso fields (grey arrows). The pink circle denotes the core of the region, where Madeira Mode Water (MMW) is formed by winter convection of Subtropical Eastern North Atlantic Central Water (ENACW_T). Yellow-shaded area denotes possible interaction or exchange between the Gulf of Cadiz Current (GCC) and AC-origin meander. Open crossed circles denote the region of central water (CW) entrainment. Legend in italics denotes information obtained from the literature (Pérez et al., 2009). (For interpretation of the references to colour in this figure legend, the reader is referred to the web version of this article.)

- 0.1 Sv of ENACW_T from the north of the box: 0.38 Sv that reaches the Gulf of Cadiz in the Gulf of Cadiz current, minus 0.3 Sv that flows in the Gulf of Cadiz Current into the Mediterranean Sea (according to Pérez et al., 2009);
- 0.22 Sv of ENACW_T from the AC: 0.72 Sv that is available to reach the Gulf of Cadiz in the AC current minus 0.5 Sv of offshore central water flowing into the Mediterranean Sea (according to Pérez et al., 2009).

The total entrainment is thus 0.8 Sv; if we also consider the 0.3 Sv of ENACW_T being downwelled and pulled out of the box by MW, the total amount of central water being subducted would be 1.1 Sv. Addition of this entrained central water to the 0.77 Sv of MOW results in ~1.6 Sv of MW, in good agreement with Alves et al. (2011).

Another way of evaluating whether 1.6 Sv is a confident value is from the straightforward salinity balance of the water masses involved in MW formation. On the one hand, ENACW_T crosses the northern limits of our box with a mean salinity of 35.82 psu; on the other hand, ENACW_T conveyed by the AC has a higher mean salinity of 36.0 psu. ENACW_T from both sources is expected to increase in salinity by net evaporation on its way to the Gulf of Cadiz region. Indeed, Atlantic surface water reaching the Gulf of Cadiz is known to have a mean salinity of 36.4 psu (Huertas et al., 2009). On the other hand, ENACW_p entering the northern section has a mean salinity of 35.73 psu. As it flows southwards off the Portuguese coast, its salinity is expected to increase by diapycnal mixing with the underlying MW (van Aken, 2000). Therefore, and in view of the upper and lower limits of the straight ENACW line given by Alves et al. (2011), we took the mean salinity values representative for both central waters in the Gulf of Cadiz region as 36.4 psu for ENACW_T and 35.62 psu for ENACW_p. In addition, we chose 38.4 psu for the MOW (as given by García-LaFuente et al., 2011). The final MW formation rate can be approximated from:

$$\frac{T_{MOW} * S_{MOW} + T_{ENACW_T} * S_{ENACW_T} + T_{ENACW_p} * S_{ENACW_p}}{S_{MW}} = \frac{(0.77 \times 38.4) + (0.3 \times 36.4) + (0.5 \times 35.62)}{36.5} \approx 1.6 \text{ Sv of MW}$$

The value estimated from this simple decomposition matches the net MW transport obtained from inversion, within the error bars (-1.48 ± 0.4 Sv). Note that if we include the incoming net AA transport across the limits of CAIBOX (0.14 ± 0.6 Sv, 35 psu) as a component of MW formation, the resulting MW volume would increase slightly to 1.7 Sv. We did not include this transport into the above estimate, for this quasi-synoptic point of view, because this water mass suffers a high degree of erosion as it spreads northwards.

Concluding remarks

Data from a new quasi-synoptic section investigated in the Iberian Basin–Canary Island region during summer 2009 were used to derive and describe the full-depth circulation field by means of a box inverse model. The SADCPC data provided a good comparison to check the robustness of our geostrophic solution. The most remarkable results are summarized below.

1. Quasi-synoptic-derived transport for the main currents within the limits of the CAIBOX AC–ACC system were as follows:
 - The AC crosses the western section (20°W) between 34.3 and 35.7°N and transports 13.1 ± 2.5 Sv. This current is the main source of heat (0.7 ± 0.1 PW) and salt (470 ± 88 Sv psu) in the region.
 - North of the AC, the ACC is centred at ~600 dbar, between 37.74 and 39.24°N. ACC transport (disregarding the influence of the AC-derived eddy) is -5.2 ± 2.1 Sv, indicating an AC:ACC ratio of 2.5.

- The CC flows south-westwards, centred at 0–600 m depth, with a net transport of 7.1 ± 1.1 Sv. This value is higher than those reported in the literature for this period of the year and corresponds to strengthening of the eastern southward branch of the subtropical gyre (McCarthy et al., 2012; Pérez-Hernández et al., 2013). This current comes from recirculation of the AC, as $\sim 54\%$ of the AC recirculates into the CC.
 - PC transport was computed as net transport across the northern section, from 18°W onshore and between surface and 800 m depth, with a value of 4.5 ± 1.4 Sv.
2. MW exportation was refined during a quasi-synoptic summer cruise involving a closed box west of the Gibraltar Strait to a value of $\sim 1.5 \pm 0.4$ Sv. This water mass is the main exporter of salt and heat out of the box (-0.6 ± 0.08 PW, -54 ± 16 Sv psu); 0.95 ± 0.7 Sv of the total MW exportation flows northwards, with a maximum contribution of 84%. This contribution accounts for the degree of dilution of the water mass from its area of formation (100% being the pure water type). The westward vein is a more diluted form of MW (maximum contribution, 62%). The increase in contribution over that reported in previous studies (Álvarez et al., 2005) indicates that MW at its source in the Gulf of Cadiz is becoming saltier and warmer due to warming and salinification of the central waters that are entrained. The spread of this water mass from the Gulf of Cadiz region towards the Atlantic Ocean corresponds to a (northward: westward: southward) ratio of 65:32:3, similar to that obtained from summer climatological data (58:29:13).
 3. Overturning into the region was estimated at 1.7 Sv, with ENACW_T accounting for part of the upper incoming limb and MW part of the outflowing lower limb. Recirculation of ENACW_T out of the box at 0.3 Sv above the MW level leads us to conclude that not only is central water transformed into MW, with flow across the Gibraltar Strait, but there is downwelling to outflow without mixing with MOW.
 4. New insights into overturning circulation were obtained from the origin of the central water involved in entrainment. Of the ENACW_P entering the box across the northern section and the north-west corner, 60% recirculates anticyclonically in the ACC westward jet, while 20% continues flowing southwards to join the CC. The remaining 20% is the volume available to take part in MW formation (Gulf of Cadiz) or central water inflow into the Mediterranean Sea (Gibraltar Strait). Of the ENACW_T entering the box, mainly through the western section (net AC–ACC system), 80% recirculates into the CC, while 10% is estimated to be transformed into MMW, and the remaining 10% is the volume available to flow towards the Gibraltar Strait region.
 5. Although quasi-synoptic cruises always involve highly meso-scale variation and increased horizontal salt transport, our results agree reasonably well those for geostrophic circulation derived from climatological data (always within the range of the error).

Acknowledgements

This work is part of the CAIBEX Project: *Shelf-ocean exchanges in the Canaries-Iberia large marine ecosystem* (CTM2007-66408-CO2/MAR), supported by the Spanish Council of Education and Science. The authors thank the cruise participants, both the *Sarmiento de Gamboa* crew and the scientific and technical team, for their indispensable help, to X.A. Álvarez-Salgado and V. Viéitez dos Santos for providing the nutrient data and to N. Fajar for the O₂ data. Thank you very much in particular to Ms Elisabeth Heseltine for her valuable help with the English review. Finally, we thank the editor and the two anonymous reviewers for their helpful comments and

suggestions, which greatly improved the original manuscript. The first author, L.I.C., was first funded by a predoctoral fellowship FPU from the Formation National Programme of Human Resources, within the framework of the National Plan for Scientific Investigation, Development and Technological Innovation 2008–2011, from the Spanish Council of Education, and now is funded by the Spanish Research Council, through the 7th Framework Program (EU FP CARBOCHANGE, C_ENVIR/0869).

References

- Álvarez, M., Bryden, H.L., Pérez, F.F., Ríos, A.F., Rosón, G., 2002. Physical and biogeochemical fluxes and net budgets in the subpolar and temperate North Atlantic. *Journal of Marine Research* 60, 191–226. <http://dx.doi.org/10.1357/00222400260497462>.
- Álvarez, M., Pérez, F.F., Shoosmith, D.R., Bryden, H.L., 2005. Unaccounted role of Mediterranean Water in the drawdown of anthropogenic carbon. *Journal of Geophysical Research* 110, C09S03. <http://dx.doi.org/10.1029/2004JC002633>.
- Álvarez, M., Álvarez-Salgado, X.A., 2007. Biogeochemical budgets in the eastern boundary current system of the North Atlantic: evidence of net heterotrophy and nitrogen fixation. *Limnology and Oceanography* 52, 1287–1292.
- Álvarez-Salgado, X.A., Fraga, F., Pérez, F., 1992. Determination of nutrient salts by automatic methods both in seawater and brackish water: the phosphate blank. *Marine Chemistry* 39, 311–319.
- Álvarez, M., Álvarez-Salgado, X.A., 2009. Chemical tracer transport in the eastern boundary current system of the North Atlantic. *Ciencias Marinas* 35 (2), 123–139.
- Álvarez-Salgado, X.A., Rosón, G., Pérez, F.F., Pazos, Y., 1993. Hydrographic Variability off the Rías Baixas (NW Spain) during the upwelling season. *Journal of Geophysical Research* 98, 14447–14455. <http://dx.doi.org/10.1029/93JC00458>.
- Álvarez-Salgado, X.A., Figueiras, F.G., Pérez, F.F., Groom, S., Nogueira, E., Borges, A.V., Chou, L., Castro, C.G., Moncoiffé, G., Ríos, A.F., Miller, A.E., Frankignoulle, M., Savidge, G., Wollast, R., 2003. The Portugal coastal counter current off NW Spain: new insights on its biogeochemical variability. *Progress in Oceanography* 56, 281–321. [http://dx.doi.org/10.1016/S0079-6611\(03\)00007-7](http://dx.doi.org/10.1016/S0079-6611(03)00007-7).
- Alves, M., Gaillard, F., Sparrow, M., Knoll, M., Giraud, S., 2002. Circulation patterns and transport of the Azores Front-Current system. *Deep Sea Research Part II: Topical Studies in Oceanography* 49, 3983–4002.
- Alves, J.M.R., Carton, X., Ambar, I., 2011. Hydrological structure, circulation and water mass transport in the Gulf of Cadiz. *International Journal of Geosciences* 2, 432–456. <http://dx.doi.org/10.4236/ijg.2011.24047>.
- Anderson, L.A., Sarmiento, J.L., 1994. Redfield ratios of remineralization determined by nutrient data analysis. *Global Biogeochemistry Cycles* 8, 65–80. <http://dx.doi.org/10.1029/93GB03318>.
- Arhan, M., Colin De Verdière, A., Mémy, L., 1994. The eastern boundary of the subtropical North Atlantic. *Journal of Physical Oceanography* 24, 1295–1316.
- Aristegui, J., Álvarez-Salgado, X.A., Barton, E.D., Figueiras, F.G., Hernández-León, S., Roy, C., Santos, A.M.P., 2004. The Global Coastal Ocean: Interdisciplinary Regional Studies and Syntheses. *Oceanography and Fisheries of the Canary Current/Iberian Region of the Eastern North Atlantic*. In: *The Sea: Ideas and observations on progress in the study of the Seas*. Harvard University Press, pp. 877–931, Chapter 23.
- Aristegui, J., Barton, E.D., Álvarez-Salgado, X.A., Santos, A.M.P., Figueiras, F.G., Kifani, S., Hernández-León, S., Mason, E., Machú, E., Demarcq, H., 2009. Sub-regional ecosystem variability in the Canary Current upwelling. *Progress in Oceanography* 83, 33–48. <http://dx.doi.org/10.1016/j.pocean.2009.07.031>.
- Armi, L., Zenk, W., 1984. Large lenses of highly saline mediterranean water. *Journal of Physical Oceanography* 14, 1560–1576.
- Barton, E.D., 1998. The Global Coastal Ocean: Interdisciplinary Regional Studies and Syntheses. Eastern Boundary of the North Atlantic: Northwest Africa and Iberia. In: *The Sea: Ideas and Observations on progress in the study of the Seas* (Chapter 22).
- Barton, E.D., 2001. Canary and Portugal Currents. In: *Encyclopaedia of Ocean Sciences*. Elsevier, pp. 380–389.
- Batteen, M.L., Martínez, J.R., Bryan, D.W., Buch, E.J., 2000. A modelling study of the coastal eastern boundary current system off Iberia and Morocco. *Journal of Geophysical Research* 105 (C6), 14173–14195.
- Boyer, T.P., Antonov, J.I., Baranova, O.K., Garcia, H.E., Johnson, D.R., Locarnini, R.A., Mishonov, A.V., Seidov, D., Smolyar, I.V., Zweng, M.M., 2009. In: *Levitus, S. (Ed.), World Ocean Database 2009, Chapter 1: Introduction*. Washington, D. C.
- Bozec, A., Lozier, M.S., Chassignet, E.P., Halliwell, G.R., 2011. On the variability of the Mediterranean Outflow Water in the North Atlantic from 1948 to 2006. *Journal of Geophysical Research* 116, C09033. <http://dx.doi.org/10.1029/2011JC007191>.
- Carracedo, L.I., Pardo, P.C., Villaceros-Robineau, N., De la Granda, F., Gilcoto, M., Pérez, F.F., 2012. Temporal changes in the water mass distribution and transports along the 20°W CAIBOX section (NE Atlantic). *Ciencias Marinas* 38, 263–286.
- Carracedo, L.I., Gilcoto, M., Mercier, H., Pérez, F.F., 2014. Seasonal dynamics in the Azores-Gibraltar Strait region: a climatologically-based study. *Progress in Oceanography* 122, 116–130.
- Carton, X., Danialt, N., Alves, J., Cherubin, L., Ambar, I., 2010. Meddy dynamics and interaction with neighboring eddies southwest of Portugal: Observations and

- modelling. *Journal of Geophysical Research* 115. <http://dx.doi.org/10.1029/2009JC005646>.
- Castro, C.G., Pérez, F.F., Álvarez-Salgado, X.A., Rosón, G., Ríos, A.F., 1994. Hydrographic conditions associated with the relaxation of an upwelling event off the Galician coast (NW Spain). *Journal of Geophysical Research* 99, 5135–5147. <http://dx.doi.org/10.1029/93JC02735>.
- Castro, C., Perez, F.F., Álvarez-Salgado, X.A., Fraga, F., 2000. Coupling between the thermohaline, chemical and biological fields during two contrasting upwelling events off the NW Iberian Peninsula. *Continental Shelf Research* 20, 189–210. [http://dx.doi.org/10.1016/S0278-4343\(99\)00071-0](http://dx.doi.org/10.1016/S0278-4343(99)00071-0).
- Comas-Rodríguez, I., Hernández-Guerra, A., Fraile-Nuez, E., Martínez-Marrero, A., Benítez-Barrios, V.M., Pérez-Hernández, M.D., Vélez-Belchí, P., 2011. The Azores Current System from a meridional section at 24.5°W. *Journal of Geophysical Research* 116, C09021. <http://dx.doi.org/10.1029/2011JC007129>.
- Cromwell, D., Challenor, P.G., New, A.L., 1996. Persistent westward flow in the Azores Current as seen from altimetry and hydrography. *Journal of Geophysical Research* 101, 11923–11933.
- Daniault, N., Mazé, J.P., Arhan, M., 1994. Circulation and mixing of Mediterranean Water west of the Iberian Peninsula. *Deep Sea Research Part I: Oceanographic Research Papers* 41, 1685–1714.
- Dickson, R., Gould, W., Müller, T., Maillard, C., 1985. Estimates of the mean circulation in the deep (>2000m) layer of the Eastern North Atlantic. *Progress in Oceanography* 14, 103–127.
- Fajar, N.M., Pardo, P.C., Carracedo, L., Vázquez-Rodríguez, M., Ríos, A.F., Pérez, F.F., 2012. Trends of anthropogenic CO₂ along 20°W in the Iberian Basin. *Ciencias Marinas* 38, 287–306. <http://dx.doi.org/10.7773/cm.v38i1B.1810>.
- Fraile-Nuez, E., Machín, F., Vélez-Belchí, P., López-Laatzén, F., Borges, R., Benítez-Barrios, V., Hernández-Guerra, A., 2010. Nine years of mass transport data in the eastern boundary of the North Atlantic Subtropical Gyre. *Journal of Geophysical Research* 115, C09009. <http://dx.doi.org/10.1029/2010JC006161>.
- Fusco, G., Artale, V., Cotroneo, Y., Sannino, G., 2008. Thermohaline variability of Mediterranean Water in the Gulf of Cadiz, 1948–1999. *Deep Sea Research Part I: Oceanographic Research Papers* 55, 1624–1638. <http://dx.doi.org/10.1016/j.dsr.2008.07.009>.
- Ganachaud, A., 2003. Error budget of inverse box models: The North Atlantic. *Journal of Atmospheric and Oceanic Technology* 20, 1641–1655.
- García-Lafuente, J., Sánchez-Román, A., Naranjo, C., Sánchez-Garrido, J.C., 2011. The very first transformation of the Mediterranean outflow in the Strait of Gibraltar. *Journal of Geophysical Research* 116, C07010. <http://dx.doi.org/10.1029/2011JC006967>.
- Gourcuff, C., Lherminier, P., Mercier, H., Le Traon, P.Y., 2011. Altimetry combined with hydrography for ocean transport estimation. *Journal of Atmospheric and Oceanic Technology* 28, 1324–1337. <http://dx.doi.org/10.1175/2011JTECHO818.1>.
- Haynes, R., Barton, E.D., 1990. A poleward flow along the Atlantic coast of the Iberian Peninsula. *Journal of Geophysical Research* 95 (C7), 11425–11441.
- Hernández-Guerra, A., Fraile-Nuez, E., Borges, R., López-Laatzén, F., Vélez-Belchí, P., Parrilla, G., Müller, T.J., 2003. Transport variability in the Lanzarote passage (eastern boundary current of the North Atlantic subtropical Gyre). *Deep-Sea Research Part I: Oceanographic Research Papers* 50, 189–200.
- Hernández-Guerra, A., Fraile-Nuez, E., López-Laatzén, F., Martínez, A., Parrilla, G., Vélez-Belchí, P., 2005. Canary Current and North Equatorial Current from an inverse box model. *Journal of Geophysical Research* 110, C12019. <http://dx.doi.org/10.1029/2005JC003032>.
- Huertas, I.E., Ríos, A.F., García-Lafuente, J., Makaoui, A., Rodríguez-Gálvez, S., Sánchez-Román, A., Orbi, A., Ruiz, J., Pérez, F.F., 2009. Anthropogenic and natural CO₂ exchange through the Strait of Gibraltar. *Biogeosciences* 6, 647–662.
- Huertas, I.E., Ríos, A.F., García-Lafuente, J., Navarro, G., Makaoui, A., Sánchez-Román, A., Rodríguez-Gálvez, S., Orbi, A., Ruiz, J., Pérez, F.F., 2012. Atlantic forcing of the Mediterranean oligotrophy. *Global Biogeochemical Cycles* 26. <http://dx.doi.org/10.1029/2011GB004167>, GB2022.
- Iorga, M.C., Lozier, M.S., 1999. Signatures of the Mediterranean outflow from a North Atlantic climatology: 1. Salinity and density fields. *Journal of Geophysical Research: Oceans* 104, 25985–26009.
- Jackett, D., McDougall, T., 1997. A neutral density variable for the world's oceans. *Journal of Physical Oceanography* 27, 237–263.
- Jia, Y., 2000. Formation of an Azores Current due to Mediterranean overflow in a modeling study of the North Atlantic. *Journal of Physical Oceanography* 30, 2342–2358.
- Jia, Y., Coward, A.C., de Cuevas, B.A., Webb, D.J., Drijfhout, S.S., 2007. A model analysis of the behavior of the mediterranean water in the North Atlantic. *Journal of Physical Oceanography* 37, 764–786.
- Johnson, J., Stevens, I., 2000. A fine resolution model of the eastern North Atlantic between the Azores, the Canary Islands and the Gibraltar Strait. *Deep-Sea Research I* 47, 875–899.
- Josey, S.A., Kent, E.C., Taylor, P.K., 1998. The Southampton Oceanography Centre (SOC) Ocean – Atmosphere Heat, Momentum and Freshwater Flux Atlas. Southampton Oceanography Centre Report No. 6, 30.
- Kida, S., Price, J.F., Yang, J., 2008. The upper-oceanic response to overflows: a mechanism for the Azores current. *Journal of Physical Oceanography* 38, 880–895. <http://dx.doi.org/10.1175/2007JP03750.1>.
- Le Bot, P., Kermabon, C., Lherminier, P., Gaillard, F., 2011. Cascade V6.1: A Matlab Software to Process Vessel-Mounted ADCP Data – Laboratoire de Physique des Océans. Ifremer, Centre de Brest (France).
- Lherminier, P., Mercier, H., Gourcuff, C., Álvarez, M., Bacon, S., Kermabon, C., 2007. Transports across the 2002 Greenland-Portugal Ovide section and comparison with 1997. *Journal of Geophysical Research* 112, C07003. <http://dx.doi.org/10.1029/2006JC003716>.
- Lherminier, P., Mercier, H., Huck, T., Gourcuff, C., Perez, F.F., Morin, P., Sarafanov, A., Falina, A., 2010. The Atlantic Meridional Overturning Circulation and the subpolar gyre observed at the A25-OVIDE section in June 2002 and 2004. *Deep Sea Research Part I: Oceanographic Research Papers* 57, 1374–1391. <http://dx.doi.org/10.1016/j.dsr.2010.07.009>.
- Louarn, E., Morin, P., 2011. Antarctic intermediate water influence on Mediterranean Sea water outflow. *Deep Sea Research Part I: Oceanographic Research Papers* 58, 932–942. <http://dx.doi.org/10.1016/j.dsr.2011.05.009>.
- Lux, M., Mercier, H., Arhan, M., 2001. Interhemispheric exchanges of mass and heat in the Atlantic Ocean in January–March 1993. *Deep Sea Research Part I: Oceanographic Research Papers* 48, 605–638.
- Machín, F., Hernández-Guerra, A., Pelegrí, J.L., 2006. Mass fluxes in the Canary Basin. *Progress in Oceanography* 70, 416–447. <http://dx.doi.org/10.1016/j.pcean.2006.03.019>.
- Machín, F., Pelegrí, J.L., 2009. Northward penetration of Antarctic intermediate water off Northwest Africa. *Journal of Physical Oceanography* 39, 512–535.
- Machín, F., Pelegrí, J.L., Fraile-Nuez, E., Vélez-Belchí, P., López-Laatzén, F., Hernández-Guerra, A., 2010. Seasonal flow reversals of intermediate waters in the Canary current system east of the Canary Islands. *Journal of Physical Oceanography* 40, 1902–1909.
- Mason, E., Colas, F., Molemaker, J., Shchepetkin, A.F., Troupin, C., McWilliams, J.C., Sangrà, P., 2011. Seasonal variability of the Canary Current: a numerical study. *Journal of Geophysical Research* 116, C06001. <http://dx.doi.org/10.1029/2010JC006665>.
- Mazé, J.P., Arhan, M., Mercier, H., 1997. Volume budget of the eastern boundary layer off the Iberian Peninsula. *Deep Sea Research Part I: Oceanographic Research Papers* 44, 1543–1574.
- McCarthy, G., Frajka-Williams, E., Johns, W.E., Baringer, M.O., Meinen, C.S., Bryden, H.L., Rayner, D., Duchez, A., Roberts, C., Cunningham, S.A., 2012. Observed interannual variability of the Atlantic meridional overturning circulation at 26.5°N. *Geophysical Research Letters* 39, L19609. <http://dx.doi.org/10.1029/2012GL052933>.
- McCartney, M.S., Bennett, S.L., Woodgate-Jones, M.E., 1991. Eastward flow through the mid-Atlantic ridge at 11°N and its influence on the Abyss of the Eastern Basin. *Journal of Physical Oceanography* 21, 1089–1121.
- McCartney, M.S., 1992. Recirculating components to the deep boundary current of the Northern North Atlantic. *Progress in Oceanography* 29, 283–383.
- McDowell, S.E., Rossby, H.T., 1978. Mediterranean water: an intense mesoscale Eddy off the Bahamas. *Science* 202, 1085–1087.
- Mercier, H., 1986. Determining the general circulation of the ocean: a nonlinear inverse problem. *Journal of Geophysical Research Oceans* 91, 5103–5109.
- Mercier, H., Ollivault, M., Le Traon, P.Y., 1993. An inverse model of the North Atlantic general circulation using Lagrangian float data. *Journal of Physical Oceanography* 23, 689–715.
- Mercier, H., Arhan, M., Lutjeharms, J.R., 2003. Upper-layer circulation in the eastern Equatorial and South Atlantic Ocean in January–March 1995. *Deep Sea Research Part I: Oceanographic Research Papers* 50, 863–887. [http://dx.doi.org/10.1016/S0967-0637\(03\)00071-2](http://dx.doi.org/10.1016/S0967-0637(03)00071-2).
- Müller, T., Siedler, G., 1992. Multi-year current time series in the eastern North Atlantic Ocean. *Journal of Marine Research* 50, 63–98.
- Navarro-Pérez, E., Barton, E.D., 2001. Seasonal and interannual variability of the Canary Current. *Scientia Marina* 65, 205–213.
- New, A.L., Jia, Y., Coulibaly, M., Dengg, J., 2001. On the role of the Azores Current in the ventilation of the North Atlantic Ocean. *Progress in Oceanography* 48, 163–194.
- Onken, R., 1993. The Azores countercurrent. *Journal of Physical Oceanography* 23, 1638–1646.
- Özgökmen, T.M., Chassignet, E.P., Rooth, C.G.H., 2001. On the connection between the Mediterranean Outflow and the Azores Current. *Journal of Physical Oceanography* 31, 461–480.
- Paillet, J., Mercier, H., 1997. An inverse model of the eastern North Atlantic general circulation and thermocline ventilation. *Deep Sea Research Part I: Oceanographic Research Papers* 44, 1293–1328.
- Paillet, J., Le Cann, B., Carton, X., Morel, Y., Serpette, A., 2002. Dynamics and evolution of a Northern Meddy. *Journal of Physical Oceanography* 32, 55–79.
- Pardo, P.C., Pérez, F.F., Velo, A., Gilcoto, M., 2012. Water masses distribution in the Southern Ocean: improvement of an extended OMP (eOMP) analysis. *Progress in Oceanography* 103, 92–105. <http://dx.doi.org/10.1016/j.pcean.2012.06.002>.
- Pelegrí, J.L., Aristegui, J., Cana, L., González-Dávila, M., Hernández-Guerra, A., Hernández-León, S., Marrero-Díaz, A., Montero, M.F., Sangrà, P., Santana-Casiano, M., 2005. Coupling between the open ocean and the coastal upwelling region off northwest Africa: water recirculation and offshore pumping of organic matter. *Journal of Marine Systems* 54, 3–37. <http://dx.doi.org/10.1016/j.jmarsys.2004.07.003>.
- Pérez, Á., Dubert, J., Haidvogel, D.B., Le Cann, B., 2003. Generation and unstable evolution of a density-driven Eastern Poleward Current: The Iberian Poleward Current. *Journal of Geophysical Research* 108 (C8), 3268. <http://dx.doi.org/10.1029/2002JC001443>.
- Pérez, Á., Dubert, J., Santos, A.M.P., Oliveira, P.B., Le Cann, B., 2005. Winter upper ocean circulation in the Western Iberian Basin—Fronts, Eddies and Poleward Flows: an overview. *Deep-Sea Research I* 52, 621–646.
- Pérez, Á., Dubert, J., Marchesiello, P., Teles-Machado, A., 2007. Surface circulation in the Gulf of Cadiz: Model and mean flow structure. *Journal of Geophysical Research* 112. <http://dx.doi.org/10.1029/2007JC004159>.

- Pérez, A., Marchesiello, P., Santos, A.M.P., Dubert, J., Teles-Machado, A., Marta-Almeida, M., Le Cann, B., 2009. Surface circulation in the Gulf of Cadiz: 2. Inflow-outflow coupling and the Gulf of Cadiz slope current. *Journal of Geophysical Research* 114. <http://dx.doi.org/10.1029/2008JC004771>.
- Pérez, F.F., Castro, C.G., Álvarez-Salgado, X.A., Ríos, A.F., 2001a. Coupling between the Iberian basin—scale circulation and the Portugal boundary current system: a chemical study. *Deep Sea Research Part I: Oceanographic Research Papers* 48, 1519–1533. [http://dx.doi.org/10.1016/S0967-0637\(00\)00101-1](http://dx.doi.org/10.1016/S0967-0637(00)00101-1).
- Pérez, F.F., Mintrop, L., Llinás, O., Glez-Dávila, M., Castro, C.G., Álvarez, M., Körtzinger, A., Santana-Casiano, M., Rueda, M.J., Ríos, A.F., 2001b. Mixing analysis of nutrients, oxygen and inorganic carbon in the Canary Islands region. *Journal of Marine Systems* 28, 183–201. [http://dx.doi.org/10.1016/S0924-7963\(01\)00003-3](http://dx.doi.org/10.1016/S0924-7963(01)00003-3).
- Pérez, F.F., Gilcoto, M., Aida, F.R., 2003. Large and mesoscale variability of the water masses and the deep chlorophyll maximum in the Azores Front. *Journal of Geophysical Research* 108. <http://dx.doi.org/10.1029/2000JC000360>.
- Pérez-Hernández, M.D., Hernández-Guerra, A., Fraile-Nuez, E., Comas-Rodríguez, I., Benítez-Barrios, V.M., Domínguez-Yanes, J.F., Vélez-Belchí, P., De Armas, D., 2013. The source of the Canary current in fall 2009. *Journal of Geophysical Research – Oceans* 118, 2874–2891. <http://dx.doi.org/10.1002/jgrc.20227>.
- Polzin, K.L., Toole, J.M., Ledwell, J.R., Schmitt, R.W., 1997. Spatial variability of turbulent mixing in the Abyssal Ocean. *Nature* 276, 93–96.
- Relvas, P., Barton, E.D., Dubert, J., Oliveira, P.B., Péliz, A., da Silva, J.C.B., Santos, A.M.P., 2007. Physical oceanography of the western Iberia ecosystem: latest views and challenges. *Progress in Oceanography* 74, 149–173.
- Richardson, P.L., Bower, A.S., Zenk, Walter, 2000. A census of Meddies tracked by floats. *Progress in Oceanography* 45, 209–250.
- Ríos, A.F., Pérez, F.F., Fraga, F., 1992. Water masses in the upper and middle North Atlantic Ocean east of the Azores. *Deep Sea Research Part A: Oceanographic Research Papers* 39, 645–658. [http://dx.doi.org/10.1016/0198-0149\(92\)90093-9](http://dx.doi.org/10.1016/0198-0149(92)90093-9).
- Saunders, P.M., 1982. Circulation in the eastern North Atlantic. *Journal of Marine Research* 40, 641–657.
- Schmitz, W.J., 1996. On the World Ocean Circulation: Volume I: Some Global Features/North Atlantic Circulation. Woods Hole Oceanographic Institution, Technical Report, 150 pp. <http://dx.doi.org/10.1575/1912/355>.
- Siedler, G., 1987. The Madeira mode water. *Journal of Physical Oceanography* 17, 1561–1570.
- Slater, D.R., 2003. The Transport of Mediterranean Water in the North Atlantic Ocean. University of Southampton, U.K.
- Smeed, D.A., McCarthy, G., Cunningham, S.A., Frajka-Williams, E., Rayner, D., Johns, W.E., Meinen, C.S., Baringer, M.O., Moat, B.I., Duchez, A., Bryden, H.L., 2013. *Ocean Sciences Discussion* 10, 1619–1645.
- Soto-Navarro, J., Criado-Aldeanueva, F., García-Lafuente, J., Sánchez-Román, A., 2010. Estimation of the Atlantic inflow through the Strait of Gibraltar from climatological and in situ data. *Journal of Geophysical Research* 115. <http://dx.doi.org/10.1029/2010JC006302>.
- Soto-Navarro, J., Criado-Aldeanueva, F., Sánchez-Garrido, J.C., García-Lafuente, J., 2012. Recent thermohaline trends of the Atlantic waters inflowing to the Mediterranean Sea. *Geophysical Research Letters* 39. <http://dx.doi.org/10.1029/2011GL049907>.
- Stommel, H., Arons, A.B., 1960. On the abyssal circulation of the world ocean—I. Stationary planetary flow patterns on a sphere. *Deep Sea Research* 6, 140–154.
- Tarantola, A., Valette, B., 1982. Generalized nonlinear inverse problems solved using the least squares criterion. *Reviews of Geophysics* 20, 219–232.
- Tomczak, M., 1981a. A multi-parameter extension of temperature/salinity diagram techniques for the analysis of non-isopycnal mixing. *Progress in Oceanography* 10, 147–171.
- Tomczak, M., 1981b. An analysis of mixing in the frontal zone of South and North Atlantic Central Water off North-West Africa. *Progress in Oceanography* 10, 173–192.
- Van Aken, H.M., 2000. The hydrography of the mid-latitude Northeast Atlantic Ocean: II: The intermediate water masses. *Deep Sea Research Part I: Oceanographic Research Papers* 47, 789–824. [http://dx.doi.org/10.1016/S0967-0637\(99\)00112-0](http://dx.doi.org/10.1016/S0967-0637(99)00112-0).
- Volkov, D.L., Fu, L.L., 2010. On the reasons for the formation and variability of the Azores Current. *Journal of Physical Oceanography* 40, 2197–2220. <http://dx.doi.org/10.1175/2010JPO4326.1>.
- Volkov, D.L., Fu, L.L., 2011. Interannual variability of the Azores Current strength and eddy energy in relation to atmospheric forcing. *Journal of Geophysical Research* 116, C11. <http://dx.doi.org/10.1029/2011JC007271>.
- Wunsch, C., 1994. Dynamically consistent hydrography and absolute velocity in the eastern North Atlantic Ocean. *Journal of Geophysical Research* 99 (C7), 14071–14090.
- Zenk, W., Armi, L., 1990. The complex spreading pattern of Mediterranean Water off the Portuguese continental slope. *Deep Sea Research Part A: Oceanographic Research Papers* 37, 1805–1823.